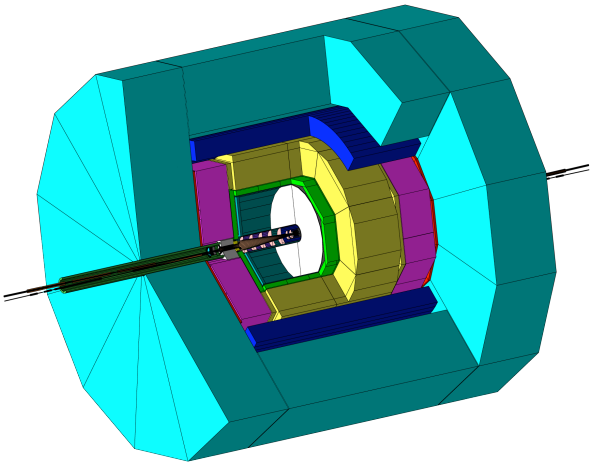

http://www-flc.desy.de/lcnotes
LC-DET-2012-067
http://ilcdoc.linearcollider.org
ILC NOTE 2012-063

The LINEAR COLLIDER TIME PROJECTION CHAMBER

of the

INTERNATIONAL LARGE DETECTOR

Report to the Desy PRC 2010

by the LCTPC Collaboration

October 2010

LC Note and ILC Note version. Built July 26, 2012

Contents

Chapter 1

Overview of the TPC for the ILD

This report was submitted to the PRC at Desy in October 2010; it contains a rather complete description of the TPC status at that time. The suggestion was made that the report should be available as LC Note and ILC Note, to be more easily accessible for the community.

The report is organized as follows. Chapter 1 serves as an executive summary of the TPC status at the time of the ILD LOI[1]. In Chapter 2, on-going R&D activities and preparations for the DBD are described in some detail. Chapter 3 gives an outlook on coming activities and concludes the report.

1.1 Motivation for the LCTPC

The subdetectors for the linear collider detector must be designed coherently to cover all possible physics channels because their roles in reconstructing these channels are highly interconnected. Two important aspects for tracking are, (a) precision-physics measurements require that the momentum of charged tracks be measured an order of magnitude more precisely than in previous experiments, and (b) high resolution measurements of the jet-energy using the particle-flow technique require efficient reconstruction of individual particles within dense jets.

A TPC as the main tracker in a linear collider experiment offers several advantages. Tracks can be measured with a large number of three-dimensional $r\phi$,z space points. The point resolution, σ_{point}, and double-hit resolution, which are moderate when compared to silicon detectors, are compensated by continuous tracking. The TPC presents a minimum amount of material X_0 as required for the best calorimeter performance. Low material budget also minimizes the effects due to the $\sim 10^3$ beamstrahlung photons per bunch-crossing which traverse the barrel region. Topological time-stamping in conjunction with inner silicon detectors is precise to $\sim$2 ns so that tracks from interactions at different bunch-crossings or from cosmics can readily be distinguished. To obtain good momentum resolution and to suppress backgrounds, the detector will be situated in a strong magnetic field of several Tesla, for which the TPC is well suited since the electrons drift parallel to $\vec{\mathrm{B}}$. The strong B-field improves σ_{point} and the two-hit resolution by compressing the transverse diffusion of the drifting electrons to $\mathcal{O}(1\text{ mm})$[2].

Continuous tracking facilitates reconstruction of non-pointing tracks, e.g. from V^0s or certain Susy (GMSB) channels, which are significant for the particle-flow measurement and in the reconstruction of physics signatures in many standard-model-and-beyond scenarios. The

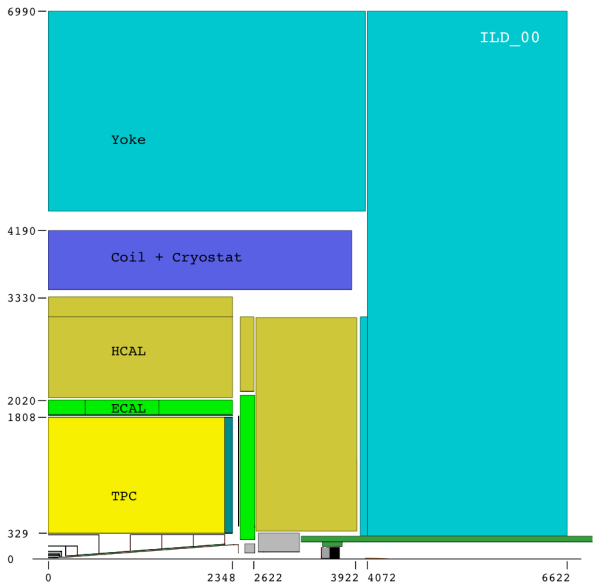

TPC gives good particle identification via the specific energy loss dE/dx which is valuable for the majority of physics analyses, e.g. for electron-π^- separation. The TPC will be designed to be robust while easy to maintain so that an endcap readout module can readily be accessed if repair is needed.

A Time Projection Chamber (TPC) is chosen for the central tracker because of its demonstrated performance in past collider experiments[3]. The main design issues at the linear collider are covered in Sec. 1.2.

1.2 Design of the LCTPC

There are important, and interconnected, design issues related to the performance, endcap, electronics, fieldcage, robustness in backgrounds, corrections and alignment. Since methods of investigating these issues have been established from past operational experience, the LCTPC groups have been actively investigating all aspects since 2001.

Performance

Main goals for the TPC performance at the linear collider are given in Table 1.1. Understanding the properties and achieving the best possible point resolution have been the object of R&D studies of Micro-Pattern Gas Detectors (MPGD), MicroMegas[4] and GEM[5] (Chapter 2), and results from this work are reflected in Table 1.1.

Endcap

The two TPC endcaps will have an area of 10 m^2 each. The readout pads, their size, geometry and connection to the electronics and the cooling of the electronics, are all highly correlated design tasks. The material of the endcap and its effect on ECAL for the particle-flow measurement in the forward direction will be minimized. However the result of a recent study is that the endcap thickness is less critical than originally thought: Table 1.2 shows how the PFA resolution changes when the endcap X_0 thickness is increased [7]. Since the LOI value of 15%X_0 turned out to be too optimistic, the goal now is to keep the endcap below 25%X_0 so that there will be little change in the PFA performance.

Table 1.1: An overview of goals for performance and design parameters for an LCTPC with standard electronics.

Size	$\phi = 3.6$m, L $= 4.3$m outside dimensions
Momentum resolution (3.5T)	$\delta(1/p_t) \sim 9 \times 10^{-5}$/GeV/c TPC only ($\times$ 0.4 if IP incl.)
Momentum resolution (3.5T)	$\delta(1/p_t) \sim 2 \times 10^{-5}$/GeV/c (SET+TPC+SIT+VTX)
Solid angle coverage	Up to $\cos\theta \simeq 0.98$ (10 pad rows)
TPC material budget	~ 0.05X$_0$ including the outer fieldcage in r
	~ 0.25X$_0$ for readout endcaps in z
Number of pads/timebuckets	$\sim$ 1 - 2$\times 10^6$/1000 per endcap
Pad size/no.padrows	$\sim$ 1mm$\times$4–6mm/$\sim$200 (standard readout)
σ_{point} in $r\phi$	$< 100\mu$m (average over L$_{sensitive}$ for straight radial tracks)
σ_{point} in rz	$\sim 0.4 - 1.4$ mm (for zero–full drift)
2-hit resolution in $r\phi$	~ 2 mm (for straight radial tracks)
2-hit resolution in rz	~ 6 mm (for straight radial tracks)
dE/dx resolution	~ 5 %
Performance	$> 97\%$ efficiency for TPC only (p$_t >$ 1GeV/c), and
	$> 99\%$ all tracking (p$_t >$ 1GeV/c)[6]
Background robustness	Full efficiency with 1% occupancy,
	simulated for example in Fig. 1.3(right)
Background safety factor	Chamber will be prepared for 10 $\times$ worse backgrounds
	at the linear collider start-up

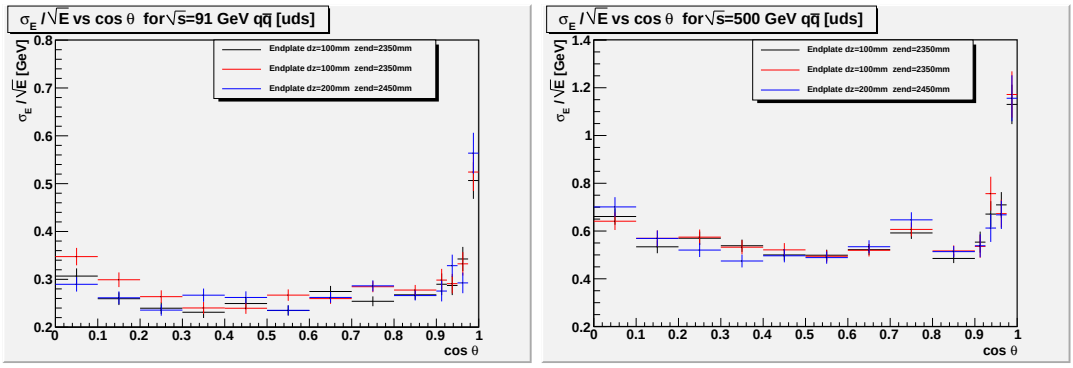

Figure 1.1: PFA performance for different endcap mechanical thicknesses.

Also the TPC endcap mechanical thickness is not critical [8], as long as the deviations from the goals are in the ballpark shown in Figs. 1.1. For the LOI, the goal for the mechanical thickness was 100 mm, whereas now it is clear that twice that value will cause no change in performance.

Table 1.2: Jet energy resolution as a function of radiation lengths in the TPC endcap region, $0.8 < cos\ \theta < 0.9$.

	45 GeV	100 GeV	250 GeV
15%X_0	0.28±0.01	0.32±0.01	0.47±0.02
30%X_0	0.30±0.01	0.31±0.01	0.47±0.02
45%X_0	0.30±0.01	0.32±0.01	0.52±0.02
60%X_0	0.32±0.01	0.33±0.01	

Designing for the finest possible granularity will minimize the occupancy arising from the TPC drift-time integrating over about 100 bunch-crossings[9]. The sensitive volume will consist of several$\times 10^9$ 3D-electronic standard-readout voxels (two orders of magnitude more than at LEP) or 10^{12} voxels in case of pixel readout. Development of the layout of the endcaps, i.e. conceptual design, stiffness, division into sectors and dead space, has started, and first ideas are shown below (Secs. 2.3.1 and 2.3.2).

Electronics

For the readout electronics, one of the important questions is the density of pads that can be accommodated while maintaining a stiff, thin, coolable endcap. The options being studied are (1) standard readout of several million pads or (2) pixel readout of a thousand times more pads using CMOS techniques. Table 1.1 assumes standard readout electronics; a similar table for pixel electronics will be made when the R&D is further advanced[10][11]. A basic ingredient for the front-end electronics will be the use of power-pulsing which is possible due to the bunch-train time structure and is assumed to give a power reduction of order 50 to 100; what can be achieved in practice is an important R&D issue (Sec. 2.3.5).

(1) Standard readout:

Small pads, $\sim$ 1mm$\times$5mm, have been found to provide good resolution from the R&D work and to guarantee the low occupancy in Table 1.1. Studies have started to establish the realistic density of pads that can be achieved on the endcap. A preliminary look at the FADC approach (à la Alice[12][13]) using 130 nm technology indicates that even smaller sizes might be feasible. In preparation for the possibility that the material budget requires larger pads, the resistive-anode charge-dispersion readout technique[14] is being studied as an option to maintain the good point resolution. Since this technique could compromise the two-track resolution and occupancy, more R&D is required.

(2) CMOS pixel readout:

The concept for the combined gas amplification and readout is under development [11][15]. In this concept the "standard" MPGD is produced in wafer post-processing technology on top of a CMOS pixel readout chip, thus forming a thin integrated device of an amplifying grid and a very high granularity endcap with all necessary readout electronics incorporated. For a readout chip with $\sim 50\mu$m pixel size, this would result in $\sim 2 \cdot 10^9$ pads ($\sim 4 \cdot 10^4$ chips) per endcap. This concept offers the possibility of pad sizes small enough to observe the individual primary electrons formed in the gas and to count the number of ionisation clusters per unit track length, instead of measuring the integrated charge collected. The R&D program (Chapter 2) will determine on what time scale this technology will become feasible for a large TPC[10].

Fieldcage

The design of the inner and outer fieldcages involves the geometry of the potential rings, the resistor chains, the central HV-membrane, the gas container and a laser system. These must be laid out to sustain $\mathcal{O}$(100kV) at the HV-membrane with a minimum of material. The goals for the inner and outer fieldcage thicknesses are about 1%X_0 and 3%X_0, respectively, while the chamber gas adds another 1%X_0. For alignment purposes a laser system is being considered and may be integrated into the fieldcage[12][16]. The non-uniformities due to the fieldcage design and fabrication can be minimized using past experience[17].

Backgrounds and robustness

The issues are the space-charge, covered in the next item below, and the track-finding efficiency in the presence of backgrounds which will be discussed here.

To start with a comment first, since heavy-ion TPCs can handle a large load of hits (Fig. 1.2 [12]), the LCTPC will be able to also since the occupancy from the linear collider will be smaller than for the heavy-ion experiments.

For e^+e^-, there are backgrounds from the collider, from cosmics or other sources and from physics events. The main source is the collider, which gives rise to gammas, neutrons and charged particles due to $\gamma\gamma$ interactions and beam-halo muons being deposited in the TPC at each bunch-crossing[10]. Simulations of the main sources[9] arising from beam-beam effects–gammas, pairs and neutrons–under nominal conditions indicate an average occupancy of the TPC of less than 0.1%, Fig. 1.3 (left top). The TPC track finding at these occupancy levels remains robust due to its continuous 3D-granularity tracking which is still inherently simple, robust and very efficient with the unoccupied remainder of as the study in Fig. 1.3(right) demonstrates. The following example underlines this conclusion.

Practical example [1]

For a conservative value for the TPC gas drift velocity, $4\,\mathrm{cm}\,\mu\mathrm{s}^{-1}$, the maximum TPC drift length of 2.25 m corresponds to 150 BXs. Nominal background in the TPC is thus simulated as 150 BXs appropriately shifted in z. Prior to the reconstruction, nearby hits are merged taking into account the expected $r\phi$ and z extent of the charge cloud. For the TPC readout assumed for ILD, 150 BXs of beam-related background correspond to a voxel occupancy of approximately 0.05 % (the TPC voxel size for this study is taken to be 1 mm in the ϕ direction, 6 mm in r and 5 mm in z). Figure 1.4 shows the TPC hits for a single $t\bar{t}$ event at $\sqrt{s} = 500\,\mathrm{GeV}$ overlayed with 150 BXs of pair-background hits. On average there are 265,000 background hits in the TPC, compared to the average number of signal hits of 23100 (8630 from charged particles with $p_T > 1\,\mathrm{GeV}$). Even with this level of background, the tracks from the $t\bar{t}$ event are clearly visible in the $r\phi$ view. A significant fraction of the background

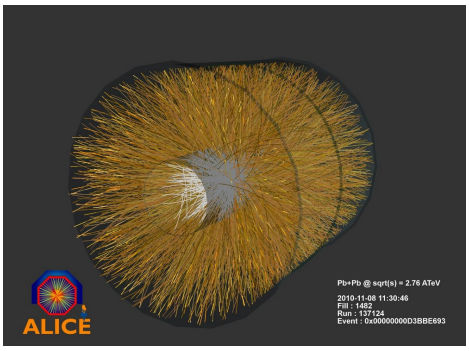

Figure 1.2: An Alice event at the LHC.

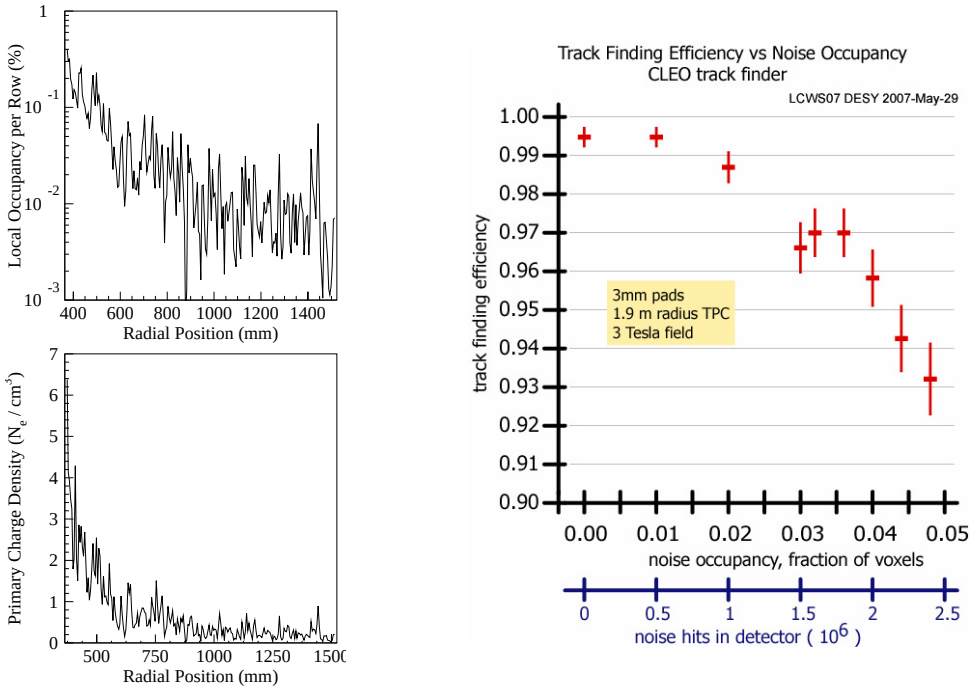

Figure 1.3: Occupancy for xyz $= 1 \times 5 \times 5\text{mm}^3$ voxels (left top) and space charge(left bottom) due to the major beam-beam effects (beamstrahlung photons, electron-positron pairs and neutrons) as simulated in [9]. Study of the tracking efficiency in the presence of backgrounds (right); this study [18] assumed a conservative voxel size of $3 \times 10 \times 40\text{mm}^3$.

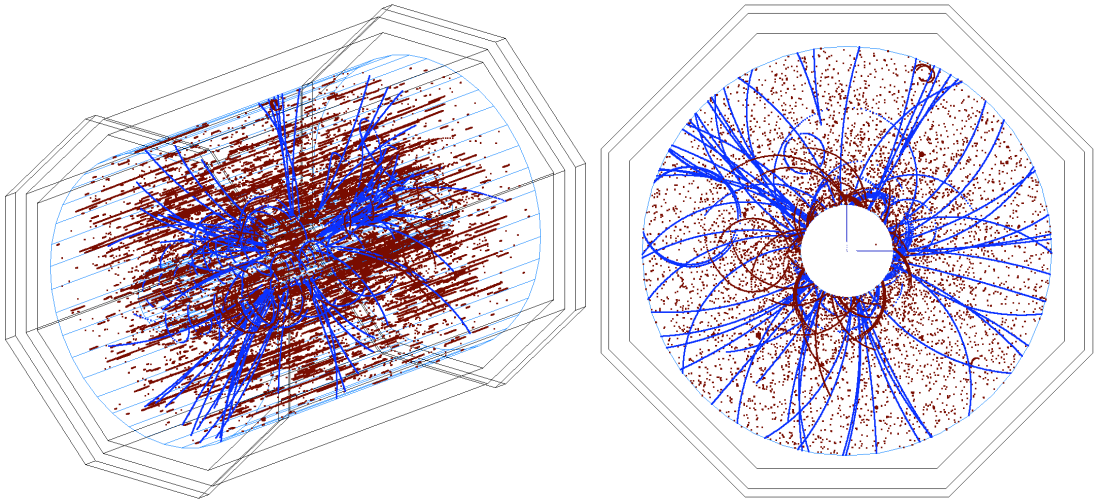

Figure 1.4: The angle and $r\phi$ views of the TPC hits from a 500 GeV $t\bar{t}$ event (blue) with 150 BXs of beam background (red) overlayed.

hits in the TPC arise from low energy electrons/positrons from photon conversions. These low energy particles form small radius helices parallel to the z axis, clearly visible as lines in the rz view. These "micro-curlers" deposit charge on a small number of TPC pads over a large number of BXs. Specific pattern recognition software has been written to identify

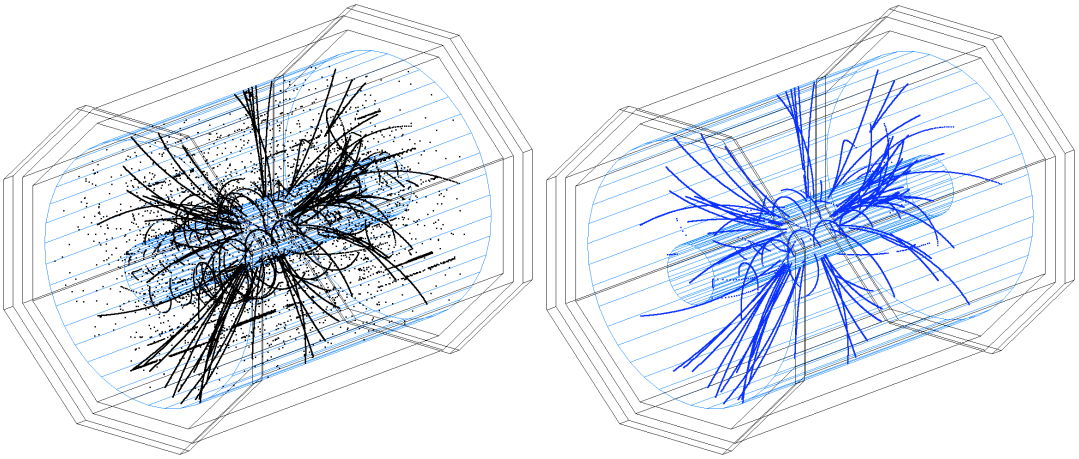

Figure 1.5: Left: The angle view with the micro-curler removal algorithm applied; this is the input to the TPC track finding algorithm. Right: the same event, now showing the reconstructed TPC tracks.

and remove these hits prior to track reconstruction. (Similar cuts are expected to remove a significant fraction of hits from beam halo muons.) Figure 1.5 (left) shows the TPC hits after removing hits from micro-curlers. Whilst not perfect, the cuts remove approximately 99 % of the background hits and only 3 % of hits from the primary interaction and the majority of these are from low p_T tracks. Less than 1 % of hits from tracks with p_T >1 GeV originating from the $t\bar{t}$ event are removed.

This level of background hits proves to be no problem for the track-finding pattern recognition software, as can be seen from Figure 1.5 (right). Even when the background level is increased by a factor of three over the nominal background no degradation of TPC track finding efficiency is observed for the 100 events simulated. This study demonstrates the robustness of TPC tracking in the ILC background environment.

Corrections for non-uniform fields

Both fields, (A) magnetic and (B) electric, can have non-uniformities which must be corrected. The (C) chamber gas will play a crucial role in minimizing corrections.

(A) Magnetic field−Revised tolerances at the ILD meeting in Paris 2010

At the ILD meeting in Paris, January 2010, the TPC group decided *NOT* to demand a non-uniformity of the magnetic field of the solenoid to within the tolerance of $\int_{\ell_{\rm drift}} \frac{B_r}{B_z} dz < 2-10$mm as used for previous TPCs, where the homogeneity had been furnished by corrector windings at the ends of the solenoid. The reason is because, at the ILC, much larger gradients (of order $\int_{\ell_{\rm drift}} \frac{B_r}{B_z} dz \sim 50$mm) will arise from the field of the anti-DID (Detector Integrated Dipole) which will be important for reducing backgrounds originating from the beams inside the detector at an IR with ±7 mrad crossing-angle. Because of the anti-homogeneity effect of the anti-DID, the original homogeneity tolerance was relinquished.

This issue was studied intensively and summarized in [19][17], where it is concluded that the TPC performance will not be degraded if the B-field is mapped to around 10^{-4} relative accuracy and the procedures outlined below (under **Alignment**) are followed. Based on past experience[19], the field-mapping gear and methods will be able to accomplish the goal of 10^{-4} for the relative accuracy, whereby the knowledge of the magnetic field must be improved beyond this initial precision. Based on the limit of the internal fit sagitta, the magnetic field

map must have a precision of $\int B_r(correction)/B_z dz \sim 30\mu$m. For the case that magnetic field distortions that are coherent along the drift length of about 2 meters, the integral is equivalent to the requirement that $dB/B < 10^{-5}$. It is envisioned that stiff tracks as observed in either Z decays or in high energy collisions will provide the necessary information (see **Alignment** below).

(B) Electric field

Three sources of space charge are (*i*) primary ion build-up in the drift volume, (*ii*) ion build-up at the readout plane and (*iii*) ion backdrift, where ions created at the readout plane could drift back into the TPC volume.

(*i*) Primary ion build-up in the drift volume. An irreducible positive-ion density due to the primary ionisation collected during about 1 s (the time it takes for an ion to drift the full length of the TPC) will be present in the drift volume. The positive-ion density will be higher near the cathode, where the local volume integrates over backgrounds from up-to-five bunch trains, and using Fig. 1.3(left bottom)[1], the charge will reach ∼1 fC/cm^3 at the inner fieldcage and ∼0.02 fC/cm^3 at the outer fieldcage. The effect of the charge density will be established by the R&D program, but the experience of the STAR TPC[16] indicates that 100 fC/cm^3 is tolerable[10], two orders of magnitude larger than expected for the LCTPC.

(*ii*) Ion build-up at the readout plane. At the surface of the gas-amplification plane during an ILC bunch train of about 3000 bunch crossings spanning 1 ms, there will be few-mm sheet layer of positive ions built up due to the gas amplification of the incoming charge followed by ion backflow. An important property of MPGDs is that they suppress naturally the backflow of ions produced in the amplification stage; studies show that this backflow can be reduced to about 0.25%[10]. Using the results from Fig. 1.3 (left bottom), this layer of readout-plane ions will attain a density of $\mathcal{O}(80)$ fC/cm^3 at the inner radius and $\mathcal{O}(2)$ fC/cm^3 at the outer radius of the TPC. Its effect will be simulated, but it should affect coordinate measurement only by a small amount since the incoming drift electrons experience this environment during only the last few mm of drift. The TPC must plan to run with the lowest possible gas gain, meaning of order $\sim 2 \times 10^3$ or less, in order to minimize this effect.

(*iii*) Ion backdrift and gating. The ion buildup described in (*ii*) will drift as an "ion sheet" back through the TPC volume unless eliminated by a gating plane. Thus an inter-train gate is foreseen to stop the ion sheets from drifting through the TPC. The ILC bunch train structure requires an open-gate operation, without intra-train gating between bunch crossings, to optimally utilize the delivered luminosity. The inter-train gate will remain open throughout one full train and be closed between bunch trains. As the ion drift velocity is much less than that of the electrons, the gate timing allows collection of all of the ions. The added amount of material for a gating plane will be small (e.g., $< 0.5\%X_0$ was the average thickness for the Aleph TPC gate).

(C) Chamber gas

The choice of the gas for the LCTPC is crucial for efficient and stable operation at the linear collider[2]. The σ_{point} resolution achievable in $r\phi$ is dominated by the transverse diffusion, which should be as small as possible; this implies that $\omega\tau$ for the gas should be large so that the transverse diffusion is compressed by the B-field. Large $\omega\tau$ means that the drifting electrons follow the B-field, which can be well measured[19][17], and has the added advantage of making the chamber less sensitive to space-charge effects and other sources of electric field non-uniformities. Simultaneously a sufficient number of ionisation electrons must be created

[1]The numbers in the text derived from this figure have been multiplied by a safety factor of two to account for other sources of backgrounds.

for the position and dE/dx measurements. The drift velocity at a drift field of at most a few times 100 V/cm should be around 5–10 cm/μs to limit the central cathode voltage and the event overlap. The choice of operating voltage must also take into account the stability of the drift velocity due to fluctuations in temperature and pressure.

Alignment

Achieving a momentum resolution an order of magnitude better than any of the collider detectors to date will be a challenge. The systematics of alignment of tracking subdetectors must be well thought through from the beginning to guarantee the integrity of tracking over a radius of two meters. Redundant tools for solving this issue are Z-peak running, the laser system, the B-field map as described in [19] and monitored by a matrix of Hall-plates/NMR-probes outside the TPC, and Si-layers inside the inner fieldcage and outside the outer fieldcage. In general based on experience at LEP[20], about 10 pb^{-1} of data at the Z peak are requested during commissioning for the alignment of the different subdetectors, and typically 1 pb^{-1} during the year may be needed depending on the backgound and operation of the linear collider machine (e.g., after push-pull or beam loss).

The strategy learned at LEP for aligning the tracking subdetectors is also applicable for the ILD. Needed to start with are: a common alignment software package for all subdetectors, the fabrication tolerances for each subdetector $\simeq$ 10–20μm internal and $\simeq$ 0.1–0.2mm external (w.r.t. the other subdetectors) and the B-field mapped to the requirements outlined in [19]. Then the steps are: first pass through a subset of data (hadronic tracks or μ pairs from Z-peak or from $\sqrt{s}$ running), each tracking detector is aligned internally; second pass, the tracking subdetectors are lined up with respect to one another using a subset of data; finally the preceeding two steps are iterated until the correct momentum for $Z \rightarrow \mu\mu$ events is achieved. Using a simple model of the track parameters dependence on alignment tolerances, the following limits for the alignment of each of the tracking sub-systems have been derived:

- coherent displacement of the VTX, 2.8 μm;
- coherent displacement of the SIT, 3.5 μm;
- coherent displacement of the SET, 6 μm; and
- coherent displacement of the TPC, 3.6 μm.

These values must be confirmed by further studies.

Chapter 2

LCTPC R&D

2.1 R&D effort for the LCTPC

2.1.1 Overview

All of the issues affecting the TPC performance are being addressed by the R&D program carried out by the LCTPC collaboration [21].

As described in the LCTPC Memerandum of Agreement, the R&D strategy is proceeding in three phases: (1) Small Prototypes (SP), (2) Large Prototypes (LP), and (3) Design.

During Phase(1), about several years of MPGD experience has been gathered, gas properties have been well measured, the best achievable point resolution is understood, the resistive-anode charge-dispersion technique has been demonstrated, CMOS pixel RO technology has been demonstrated and commissioning has started for the LP.

In addition the options of MWPC gas-amplification has been ruled out (Sec. 2.2.5) and Micromegas with standard pads has been ruled out (Sec. 2.2.3).

The Phase(2) LP and SP work is expected to take another two–three years. Regular bi-weekly WP phone meetings started in May 2006 where details for the LP design were worked out and next R&D steps developed.

The following list gives an overview of the currently envisioned timeline for completing the studies and the construction of the ILD TPC.

• 2009-12: Continue R&D on technologies at LP, SP, pursue simulations, verify performance goals covered in Sec. 1.2.

• 2009-11: Plan and do R&D on advanced endcap; power-pulsing, electronics and mechanics are critical issues.

• 2011-12: Test advanced-endcap and power-pulsing prototypes.

• 2012-18: Design and build the LCTPC.

Construction of endplates that satisfy the material requirements of the ILD, as well as the structural requirements of the TPC, will require extensive R&D. Details of preparations are presented in the following sections.

At the beginning of the period 2012-18, the selection must be made from the different technological options – GEM, MicroMegas, resistive anode, pixel, electronics, endcap structure – to establish a working model for the design of the LCTPC. This design will be used for the ILD Detailed Baseline Document in 2012 (see Secs. 2.3) and include pad segmentation, electronics, mechanics, cooling and integration, so that performance, timeline and cost can be estimated reliably.

2.2 R&D Progress

2.2.1 Large Prototype

For the consolidation phase (Sec. 2.1.1) of the R&D of the LCTPC collaboration a Large Prototype (LP) for a Time Projection Chamber was designed, built, commissioned and tested. It has been in use for the groups of the collaboration in a test beam environment at DESY since the last quarter of 2008, and a good infrastructure for the test beam environment has been established. The main components of the LP consist of
(a) the endplate (EP),
(b) the fieldcage (FC) and cathode, and
(c) the solenoid (PCMAG).
The EP will be briefly described first, then the FC and finally PCMAG.

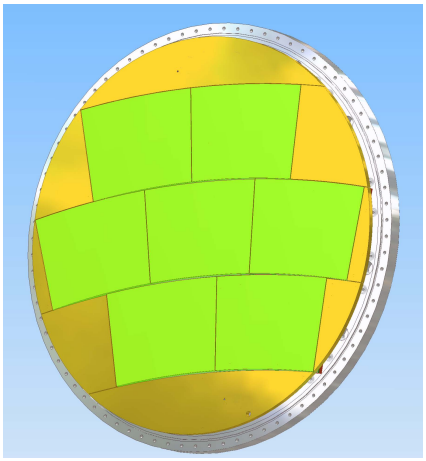

Figure 2.1: The endplate of the LP.

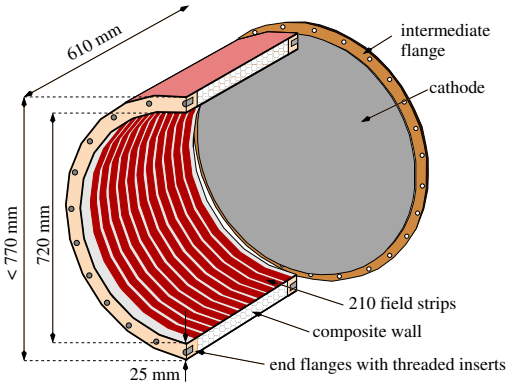

Figure 2.2: The fieldcage and cathode of the LP.

The EP. An endplate was produced that can accommodate up to seven amplification modules (Fig.2.1). The modules have identical shape and thus can be interchanged to allow for more flexibility. Since the modules do not cover the complete area of the endplate and there are not always seven modules in operation, the non-equipped parts of the endplate were positioned to have the same electric potential as the gas-amplification surface of the module(s) in operation. The non-equipped regions are mounted with termination plates and dummy modules made of bare copper planes in a module frame. A more detailed description of the EP can be found in Sec. 2.3.1.

The FC. The fieldcage [22] seen in Fig.2.2 was built in order to have a prototype that is significantly larger than the fieldcages used in smaller prototypes under study. The motivation for the size was two-fold; firstly, to have a prototype that is capable for sampling tracks with a large number of space points, and secondly, to test for the feasibility when building a fieldcage that serves both as fieldcage and as gas vessel for a TPC. The FC was designed at DESY and produced in cooperation with a company[1] that is specialized in manufacturing and processing composite materials based on fiber-reinforced plastic. The FC design required a low material budget, a robust mechanical structure and a homogeneous electric drift field.

[1]HAINDL - Individuelle Kunststoff-Verbundbauweise: www.haindl-kunststoff.de

The FC wall consists of a sandwich structure (Fig.2.3) with thickness X_{wall} =1.21±0.10% radiation lengths. The length of the FC was measured to be 610.4mm±0.1mm and the diameter of the accessible drift volume to be 720.20mm±0.07mm. The FC's barrel axis should be perpendicular to the cathode and anode, however measurements have shown that a tilt of the axis exists which results in a maximum offset of 500μm relative to the nominal position at the cathode (Fig.2.4). This tilt degrades the electric field homogeneity from $\Delta E/E \approx 10^{-4}$ to $\approx 10^{-3}$. The effect on the systematics on the track reconstruction is being investigated.

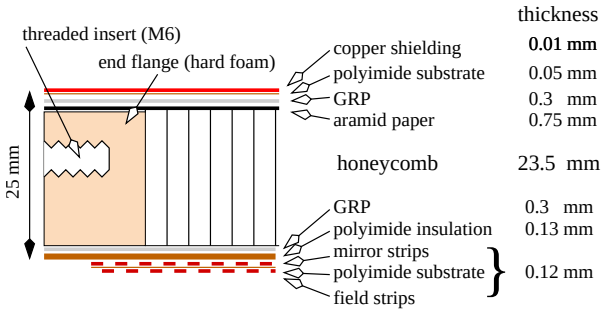

Figure 2.3: Wall structure of the FC.

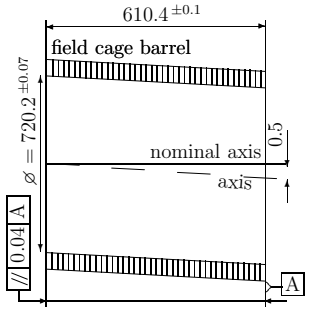

Figure 2.4: Misalignment of the FC-barrel axis.

The cathode for the LP was manufactured from an aluminum sheet of 5mm thickness. It was bonded to a thin veneer of copper (10μm) in order to produce a hole pattern when illuminated with a laser (see Sec. 2.2.6). The cathode was mounted on a set of three adjustable posts on its back side in order to align the cathode to be parallel to the anode.

The LP tolerances are such as to allow for operation with an overpressure of up to 10mbar with deformations of the structure less than a tolerance of 100μm. Finite-element calculations found that such deviations would arise with an overpressure of about 400mbar, so that the maximum overpressure of 10mbar for the ILD TPC will produce distortions well within the tolerance.

Electrical drift fields envisaged for the ILD-TPC gases could be as large as 350V/cm, corresponding to 20kV for the LP with length of about 60cm. The FC was tested to 30kV across its wall structure for 24h and no breakdown was observed, so that the FC operation for the ILD TPC should be on the safe side.

PCMAG. A superconducting magnet (PCMAG: persistent current magnet) is a coil that delivers up to 1.25T. It is usually operated at 1T with I=430A. PCMAG was developed for balloon-born experiments and has no return yoke. Consequently it has a rather inhomogeneous field distribution which also required the length of the FC to be limited to 60cm (Fig.2.5). This inhomogeneous field allows the simulation and development of correction procedures for track reconstruction. A detailed field map was produced in 2008.

Liquid He for PCMAG has been supplied from a dewar up to now, a procedure which is rather cumbersome. Now planned is to equip it with a modified cryogenic system which will recover the evaporated Helium and compresses back to the liquid phase. This is foreseen to happen in the second half of 2011.

Infrastructure. A sophisticated infrastructure for the LP has been developed and consists of equipment that is necessary in order to operate a gaseous detector according to the scientific program of the LCTPC collaboration. This includes the high voltage (HV) power supply that

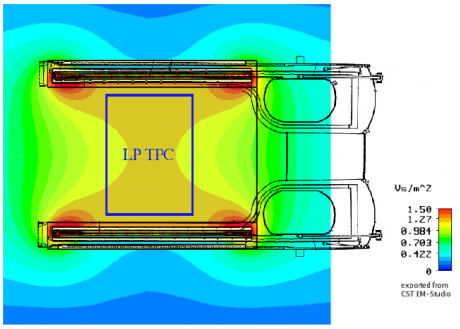

Figure 2.5: Magnetic field distribution of PCMAG, calculated with finite element methods.

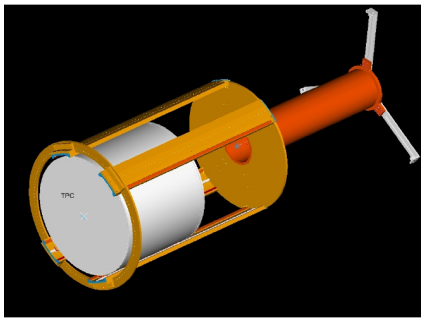

Figure 2.6: Support structure for the LP for the use within PCMAG.

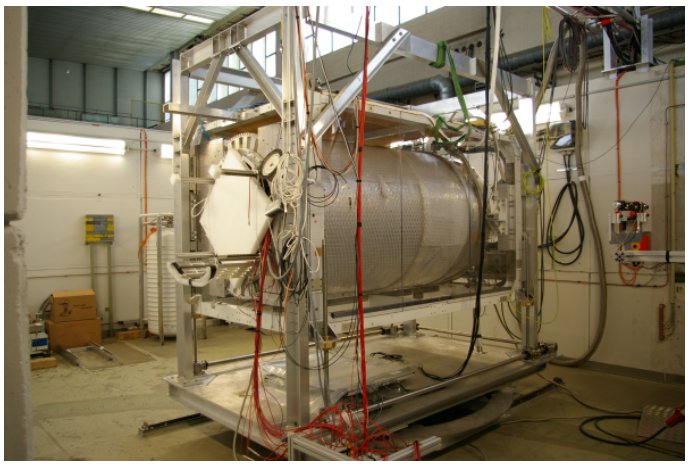

Figure 2.7: Movable stage in test beam area.

is needed for powering the FC and the individual amplification structures and a gas supply system that is capable of controlling pressure in the gas vessel by means of flow meters. The systems, HV and gas, are being monitored and the data recorded during the various data taking periods by a slow control system based on DOOCS,[2] a distributed control system that was developed for HERA and Tesla Test Facilities (TTF) applications. A support structure for the LP was constructed to fit into the bore of PCMAG (Fig.2.6) and allows the movement of the TPC along the magnet's axis.

The LP is located in a test beam environment at the DESY accelerator complex in Hamburg. In general, electrons with momenta between 1.0GeV/c $\leq$ 5.6GeV/c can be injected into the test beam area. Since the beam line is fixed with respect to the test beam area, a stage (Fig.2.7) was developed which accommodates the whole apparatus, magnet and detector system, can move the system in the vertical as well as the horizontal direction and can rotate the system in the horizontal plane. A three-fold motor system, one motor per movement controls the positioning of the detector with respect to the beam line. An independent system based on precision scales allows the measurement of the position of the stage very precisely.

Recent results. Most recently three modules of GEM detectors were installed and about

[2] doocs.desy.de

7000 channels were equipped with ALTRO readout electronics. The goals of the beam test were to measure position resolution and to perform momentum measurements in the full volume of the LCTPC large prototype. The data taking and the first preliminary analysis have been performed. For the first time tracks over the full radial distance of the LCTPC have been measured. A typical track-trigger is shown in Fig. 2.8(left) and an event with several tracks in Fig. 2.8(right).

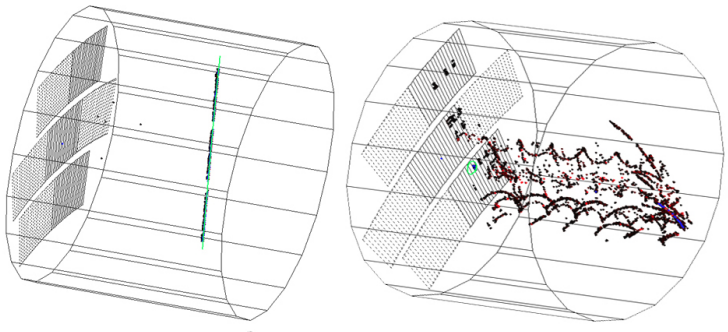

Figure 2.8: Left: GEM event with one track in the 1 T B-field. Right: GEM event where a 5 GeV/c electron hits the TPC cathode, creating many low energy particles which curl in the B-field.

2.2.2 LP with GEMs and pads

The basic concept of GEM modules is the measurement of moderately diffused electron clusters (typically 300μm) through gas amplification in GEM stacks using the corresponding fine pitch (typically 1 mm) of the pad plane in order to optimize position resolution as well as multi-track separation capability.

Two groups are working on GEM modules. (1) The Asian group is building GEM stacks by two-story 100μm-thick GEM produced by the Scienergy Company in Japan, where 100μm is chosen in order to reduce mechanical complexity and to provide enough gas gain under relaxed operation conditions for HV. This two-story structure does not have the ability to reduce the ion feedback from the gas-amplification region, so a gating device is necessary for this structure to avoid ion sheets in the TPC volume (Sec. 1.2). (2) The DESY group has started to work on building triple GEM structure using standard 50μm-thick GEMs produced by CERN. Optimizing the HV settings on the GEMS can reduce the rate of ion back-drift to 0.5% and may work under low-background conditions at the linear collider; although it may be possible to run without a gate if such a case is realizable in practice, a gating device is also planned since the running conditions are not yet known. Here we report on the Asian modules, a description of the Altro electronics follows, and developments at Desy are covered in Sec. 2.2.2.3.

2.2.2.1 Asian modules

Tests with the Asian modules will be described next.

Pad plane. The Asian pad plane for an LP module is divided into 28 pad-rows (5.4mm radial pitch) in addition to 1cm wide space at the inner-most and outer-most radii of the

module for the support frame for the GEMs, the GEM-HV supply and the gate.

A inner half and outer half pad-rows are divided into 176 pads (1.18−1.24mm in azimuthal pitch) and 192 pads (1.14−1.19mm) respectively. Each pad is routed to the back side to a 40-pin small connector placed away from the backframe to reinforce the rigidity of the PCB and to make a tight connection to the endplate. The HV lines for GEMs are also routed to the back side while keeping distance from the signal lines. Ten PCB layers are needed for these routings.

GEM structure. A 100μm thick GEM is fixed at 1cm wide frame by pillars placed at the inner and outer radii of the module and can be stretched using three adjustable screws in each place. There is no frame on both azimuthal sides with direction pointing to the interaction point in order to minimize the insensitive area. A gas gain of a few thousand is achieved with $V_{GEM} = 360V$ using this double-story structure and T2K gas (95/3/2 % Ar/CH4/Isobutane). The transfer gap between the double GEMs is set to 4mm and the induction gap to 2mm; 1 kV/cm and 2 kV/cm electric fields are applied respectively.

Gate. Originally the candidate for the gating device was an ultra-thin GEM whose thickness was 14μm and hole diameter 90μm with standard 140μm pitch. But trials showed that even a 14μm-thick GEM cannot provide enough transmission for electrons due to limited hole aperture under realistic LCTPC conditions, such as a high magnetic field and a high $\omega\tau$ gas. The current best transmission achieved in T2K gas was only 50% with 1T B field. Alternative gating devices are now under consideration, such as an ultra-large aperture GEM using new technology or a wire gate.

Beam test. Performance of a combined GEM module and ALTRO system which is described below was tested at the EUDET test beam facility on March-April 2009, March 2010 and September 2010.

The first beam test of Asian GEM module was carried out without a gating device using about 2000 readout electronics channels. The pillars which are supposed to be covered by the gating device were facing into the drift region and distorted electric field due to the missing gate. This caused a large systematic distortion due to E×B effect around the pillars. Although E×B distortions could be corrected using the measured residuals as a function of incident beam position, a rigorous evaluation of momentum resolution cannot be done with this kind of distorted data. An esitmate of the momentum resolution was obtained by applying a Kalman-filter-based track fit. The $1/P_T$ distribution had an asymmetric gaussian shape due to photon radiation from the electron beam. The resolution was estimated to be 0.083 GeV^{-1} from the symmetric part of the distribution, which is consistent with expectations, 0.081 GeV^{-1}, using the Glučkstern formula and the measured position resolution.

The second beam test was attempted with the GEM gating device, but data could not be taken due to HV problems on the module. The 14μm thick GEM gate was stretched wider than the nominal size and touched to the neighbor dummy modules. Fabrication and implementation of thin sheets require further development.

The third beam test was carried out with a field shaping cover to replace the gating device on the frame region (pillars and insulator frame); this should provide clear track data without artificial distortion from the module structure and be good enough to investigate tracking performance. The data taking took place recently, in September 2010.

Analysis tools had been developed based on YOKArawMon (Raw data monitoring software based on ROOT and upgraded to KALMAN-filtering tracking). These tracking packages have been transferred into the Marlin-TPC platform and will be used for the latest data analysis. More details on the software development is found in Sec. 2.3.6.

The goal of our LP1 test is to evaluate the tracking performance under realistic linear collider conditions including correction of non-uniform magnetic/electric fields and alignment. Achieved up to now was a demonstration that the diffusion-constant and position-resolution results, which had been measured in small prototypes, can be reproduced in the LP, as seen in Fig. 2.9.

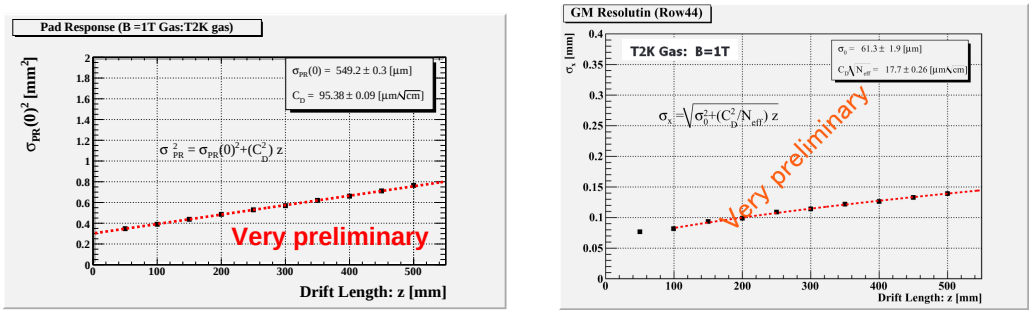

Figure 2.9: Examples of diffusion-constant (left) and point-resolution (right) measurements in the T2K gas during the recent Asian GEM test. The drift-velocity (not shown) and the diffusion-constant measurements agree with Magboltz.

2.2.2.2 Altro electronics

The Lund and CERN groups have built a readout system for the large prototype TPC which is based on the ALTRO chip, originally developed for the ALICE experiment at the LHC. The 16 channel ALTRO chip performs analogue to digital conversion with 10 bit precision followed by various steps of digital signal processing, including zero suppression and storage in an event buffer. The sampling can be clocked at frequences up to 40 MHz, and frequencies lower by multiples of two are possible. However, at 40 MHz sampling the full resolution is not maintained for the standard ALTRO chip. A limited number of ALTRO chips were modified to allow sampling at 40 MHz with almost full precision. Up to now the system has been operated during data taking at 20 MHz only. The ALTRO chip has an events storage memory of 1000 10-bit words, which corresponds to sampled data over a depth of 50 μs drift time at 20 MHz. The T2K gas mixture was used in the TPC, which gives a drift velocity of around 7 cm/μs at a drift field of 230 V/cm. This leads to a maximum drift length of 350 cm that can be accommodated in the ALTRO memory and is larger than the 60cm length of the LP.

In order to test recent technologies for gas amplification (GEMs and Micromegas for TPC readout) a new charge sensitive preamp-shaper has been developed. The programmable PCA16 chip has, as the name indicates, 16 channels and offers different choices with respect to peaking time, gain, decay time and signal polarity. The new programmable analogue chip required modifications to the Front End Card (FEC), which mainly are related to the programmability of the chip. The programming of the PCA16 chip is done remotely, and data for setting the parameter values are downloaded to the board controller FPGA on the FEC via the data bus on the back plane. An 8-bit shift register delivers the digital input to set the peaking time, the gain, the polarity and it also provides a possibility to bypass the shaping function. An octal Digital-to-Analogue Converter (DAC) controls the decay time of the output signal. The various options will make it possible to find the optimal parameter

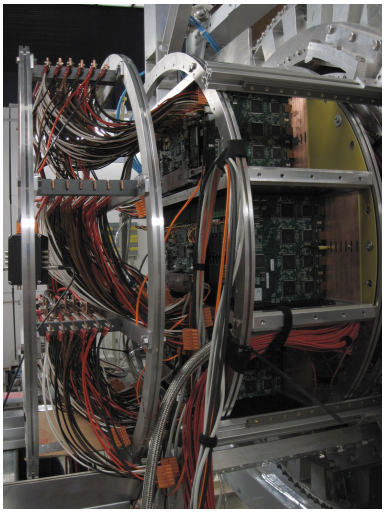

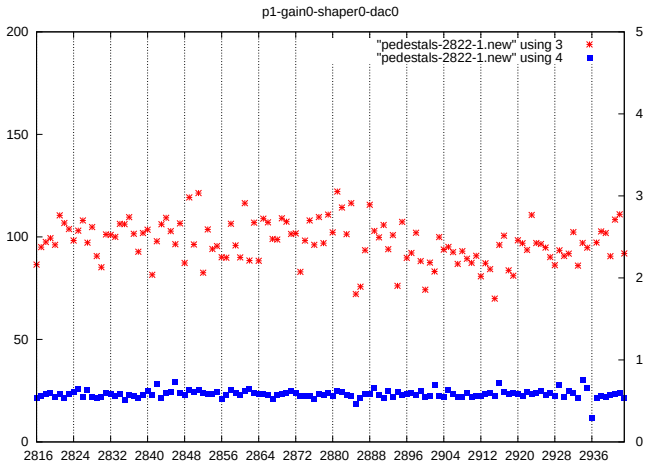

Figure 2.10: Left: The front end electronics and its support structure attached to the TPC. Also seen are the optical cables for the data readout and the LV supply cables. Right: The pedestal and noise for the different channel numbers of a FEC. The stars are the mean value of the pedestal in ADC counts (scale on left-hand ordinate); the squares are the RMS of the pedestal measurements (scale on right-hand ordinate).

settings for a given gas amplification system and for the specifications of the final chip.

Each FEC contains 128 channels i.e. 8 PCA16 chips and 8 ALTRO chips are mounted on each board. They are connected to the pad board via thin 30 cm long kapton cables. A Readout Control Unit (RCU) governs the readout of the data via a backplane to which a maximum of 32 FEC's can be inserted. Data are sent via an optical cable to a Detector Read-Out Receiver Card (DRORC), which is placed in the Data Aquisition (DAQ) PC. The DAQ software uses the ALICE drivers and libraries for communication between the DRORC and the front end electronics via the optical link. Trigger and timing control is provided by a Trigger Logic Unit (TLU), which constitutes the central trigger unit for all sub-detectors in a beam set-up and includes an event synchronization mechanism by a distributed event sequence number. A distribution box (DBOX) receives the trigger from the TLU and sends it via the RCU to the FEC's. At the reception of the trigger the ALTRO starts storing digitized information in the event buffer, up to a predefined number of samples. The RCU reads the ALTRO event buffer and sends the data on the optical link to the DRORC, which stores it in a memory in the readout computer. The DBOX blocks the trigger system so that no new events are accepted during the whole readout cycle. At the arrival of a trigger in the DBOX, it defines a time stamp of the event that is used to synchronize it with events from other detectors. The run control is done from a graphical user interface. A monitor program creates and updates histograms in a shared memory, which is also accessible from a presenter program. A photograph of a test beam set-up is shown in Fig. 2.10(left).

The electronics pedestal and noise levels for all readout channels have been measured both initially as well as on a regular basis during data taking periods, mainly for pedestal subtraction and check for corrupt channels. The front end electronics has shown excellent noise performance. A typical measurement of one FEC with the PCA16 chip programmed to provide the longest peaking time (120 ns) and the lowest gain (12 mV/fC) is presented in

Fig. 2.10(right). On the horizontal axis is given the number of the readout channel from 0 to 127 plus N*128, where N is the FEC-number, which is 22 in this case . The stars correspond to the ADC pedestal values, which can be read off on the left hand vertical scale, and the squares represent the RMS values of the pedestal measurement, which can be read off on the right hand vertical scale. The average RMS value of around 0.5 ADC counts corresponds to the equivalent noise of 260 electrons, which includes random noise, coherent clock noise and long term variations on the scale of seconds. If the gain is increased to the highest value (27 mV/fC) the noise level increases to typically about 1 ADC count, which corresponds to the equivalent noise of 231 electrons.

The ALTRO readout boards for a total of 10000 channels have now been produced and tested. It was observed during a previous test run that one of the voltage regulator chips, which supplied the voltage for the original preamplifier chip (PASA) of the ALICE electronics was undersized to provide the correct operating voltage for the PCA16 chip and had to be exchanged. The performance of the front end electronics is temperature sensitive and the chips may be damaged if the temperature gets too high. To avoid this happening and to register the board temperatures regularly, a system for monitoring the temperature has been developed and tested. A new and more efficient cooling system using compressed air has been built. Since up to 10,000 channels of readout electronics has to be housed inside the PCMAG the option of water cooling was abandoned. The DAQ system has been further improved so that it now requires less manual actions and also includes automatic shut down in case of high temperatures on the chips. For the Low Voltage (LV) supply a commercial system from Delta Elektronika has been used. The LV distribution has been modified in order to improve the access to the front end boards.

2.2.2.3 Developments at DESY

Previous measurements at DESY have shown that in a GEM TPC a pad pitch of 2.2mm is too large to reach the envisaged resolution goal of 100μm [1]. Therefore in 2008 a new set of resolution measurements in magnetic fields of up to 4T were performed with a pad pitch of $1.27 \times 7.0\text{mm}^2$.

These measurements were carried out with the MediTPC prototype [23]. A triple GEM structure was used for the gas amplification and a setup based on the ALEPH electronics for the data acquisition. The measurements were done with P5 and with T2K gases mixtures.

In Fig. 2.11, the resolution results of a measurement with P5 gas in 4T magnetic field are shown. To cross-check the results, a non-staggered (pads aligned radially) and a staggered pad plane were used in the measurements. Also, in the track reconstruction a chi-squared fit and the so-called global fit method (based on a likelihood maximization of the charge deposition)[24] were applied.

The achieved point resolution σ_x stays well below the goal of 100μm over the drift length of the prototype. Using the formula $\sigma_x^2 = D_T^2/N_{eff} + \sigma_0^2$ [25], where D_T^2 denotes the transverse diffusion constant and σ_0 the intrinsic resolution, the results were extrapolated up to 2m drift length. The results for N_{eff} and σ_0 are listed in Table 2.1. For the chi-squared fit the parameter values are comparable with results from other groups [26], while the global method yields somewhat smaller values.

The extrapolation shows that with the setup used, the diffusion is still not low enough to ensure the resolution goal of 100μm over the whole drift length of a TPC at the ILD. Even considering the reconstruction with the chi-squared method, the resolution reaches 130μm at

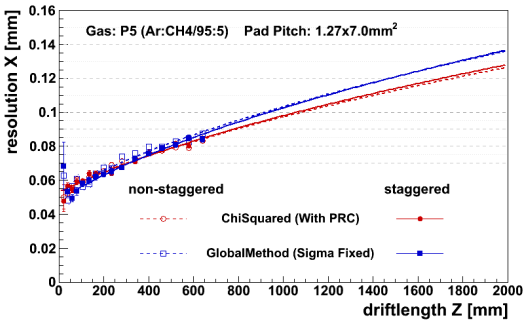

Figure 2.11: Point resolution over drift length measured with P5 gas at 4T magnetic field (cut on track angle: $\phi = 1°$) including extrapolation to 2m drift length.

Fit Method	**Pad Layout**	$\mathbf{N_{eff}}$	σ_0 [μm]
Chi Squared	non-staggered	29.4 ± 1.3	54 ± 1
Chi Squared	staggered	28.3 ± 1.2	53 ± 1
Global	non-staggered	24.4 ± 1.3	53 ± 1
Global	staggered	23.6 ± 1.1	48 ± 1

Table 2.1: Parameter results of a fit of $\sigma_x^2 = D_T^2/N_{eff} + \sigma_0^2$ to the measured point resolution for P5 gas at 4T. Only errors from the fit are given.

2m drift. However, a different gas mixture or a changed drift voltage setting could reduce the diffusion sufficiently.

Grid GEM Measurements. An analysis of surface profiles of conventionally mounted GEMs has shown that the sagging of the foils is non-negligible and of order some hundred μm [27]. These deflections yield effective gain inhomogeneities in double or triple GEM stacks and have to be avoided in order to reach the design goals of the ILD as defined in Sec. 1.2. Especially the dE/dx resolution of 5% requires a better flatness of the amplification structures. Hence, a new support structure using a ceramic grid in between the GEMs – as visible in Fig. 2.12(left) – was developed at DESY. This mounting allows for flat installation and reduces simultaneously the amount of material which has to be introduced into the detector.

Measurements with a triple grid GEM in the above-mentioned MediTPC prototype setup and P5 gas showed the utility of the grid mounting. In the direct vicinity of the grid structures the amount of charge deposited and with it the hit efficiency is reduced. A distinction between structures aligned parallel to or perpendicular to the pad rows becomes necessary, since the former does not influence the measurements, while the latter does.

The single point resolution is only slightly influenced by the grid structures in the sensitive areas of the GEMs. In Fig. 2.12(right), a comparison of a measurement run in the MediTPC with conventionally framed GEMs and grid GEMs is shown. For both cases, two methods of track fitting were used. Almost over the whole drift length, the single point resolution is smaller than 100μm. The difference between the frame and grid GEM measurement are the same order as normal run-to-run variations. More details can be found in [27].

Grid GEM Module for the Large Prototype. As a consequence of the grid GEM mea-

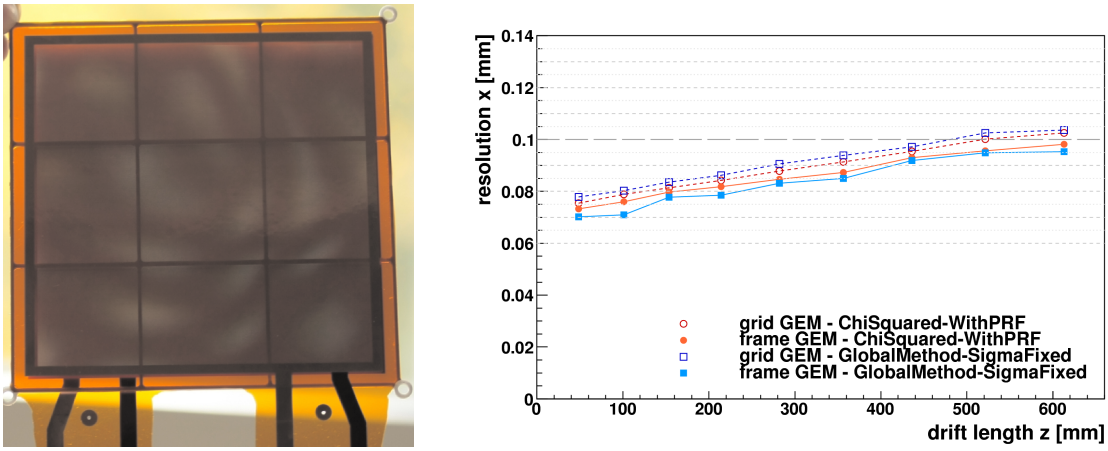

Figure 2.12: Left: Grid GEM with a sensitive surface of $10\times10\text{cm}^2$. Right: Single point resolution over drift length (cut on track angle: ϕ =0.1rad). Shown are measurements with framed GEMs and grid GEMs. For each case, two fit methods are depicted.

surements, a new module with grid GEMs for the large TPC prototype is currently under construction. This module – with its self supporting structure – will test the applicability of GEM amplification technology in large scale high energy physics detectors. In Fig. 2.13, a GEM with the grid for the module is shown. The sensitive area will be roughly of the size $17\times21\text{cm}^2$. In the planning is a triple GEM setup with an anode pad plane with pads of the

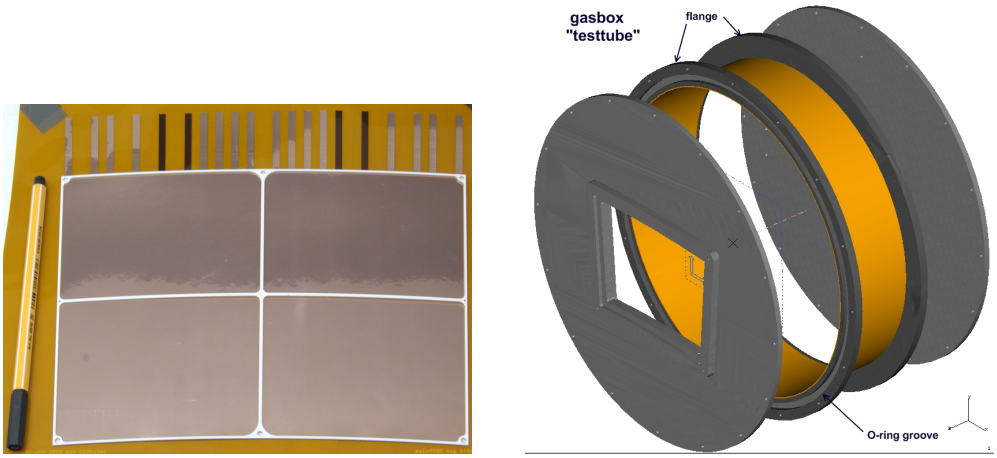

Figure 2.13: Left: Grid and GEM for a large prototype module to be built at DESY. GEM size about $17\times21\text{cm}^2$. The strips on the upper side are the HV connectors. Right: Test chamber design for the commissioning of the grid GEM module.

size of $1.26\times5.85\text{mm}^2$. But since the PCB is still in the design phase, an existing pad plane provided by the Tsinghua University will be used at first. The pads are of similar size and the connectors for the ALTRO electronics have been soldered. In addition, a powering scheme for the triple GEM is under development. In order to test and commission the module before mounting it into the LP, a dedicated test chamber will be built. The design of this chamber is shown in Fig. 2.13.

2.2.3 LP with Micromegas and large pads

Tests performed in Saclay in 2002-2004 and at KEK in 2005-2006 [28] demonstrated a satisfactory operation of a Micromegas TPC, but also showed that there is not enough spreading of the cloud charge to allow a precise determination of a center of gravity on each row. The resolution was thus limited to 200-300μm with 2mm-wide standard pads. Thus the R&D focused on the technique of the resistive anode to circumvent this limitation: a continuous 2D RC circuit is built on top of the pad array, the RC constant being tuned to spread the charge over 2-3 pads [14].

The R&D plans has proceeded in two Steps:

• Step 1. Single-module studies: five different modules were studied in succession in the central position of the LP endplate surrounded by dummy modules. The electronics designed for the T2K experiment was used to equip this module. The T2K electronics is availabile at low cost and has large flexibility: parameters such as amplifier shaping time and gain, and sampling frequency can be varied over wide ranges.

• Step 2. Multi-module studies: seven identical modules will equip the LP endplate. For this the integration of the readout had to be completely redone as explained in Sec. 2.2.3.2. The module construction benefitted from the experience gained in Step 1. A first full chain should be tested at the end of 2010, and the seven modules (plus two spares) should be ready for test at the end of 2011.

2.2.3.1 Results from Step 1.

In Step 1, five modules were tested in beam and with cosmic rays, with and without a magnetic field of 1 T. They all had the same pad geometry of roughly 3mm×7mm, with a 'keystone' shape. Due to the keystone shape of the module, the pad width varied from the innermost row to the outermost row from 2.7 to 3.2 mm. The pads were arranged in 24 rows and 72 columns. Two neighbouring pads were sacrificed to leave room for a HV connection of the mesh through the PCB. There was a 1.5 mm metal frame around the module, which can be set to the mesh HV (in the case of standard pads) or to the ground (in the case of a resistive anode).

Module 1. A standard bulk Micromegas, with 128μm pillars as in T2K. The routing, designed at CERN, was performed in eight layers.

Module 2. A resistive-ink detector: the copper pads were covered by an insulator (75μm prepreg) with a resistive-ink layer on top and connected all around the module to ground. The resistivity was estimated to be 3 MOhm/square.

Module 3. A resistive kapton detector: the copper pads were covered by a 5 MOhm/square carbon-loaded kapton foil on top of a 75μm layer of prepreg. The anode was also connected to the ground on the periphery through vias across the prepreg.

Modules 4 and 5. Two more resistive kapton detectors, with a 3 MOhm/square resistivity, were built. They differ only by the routing, one of which, designed at Saclay, is a 6-layer PCB.

All the modules performed well. One channel out of 1726 had to be disconnected in Module 1, while all the other modules were working in their entirety. All of the resistive modules never sparked. However Modules 4 and 5 were destroyed due to a short-circuit in the mesh which was traced back to a defect in the grounding of the outer ring of the resistive foil. A new technique is now used for the forthcoming fabrications. The gas used was almost always the T2K gas. The operation was free from sparking due to the resisitive coating.

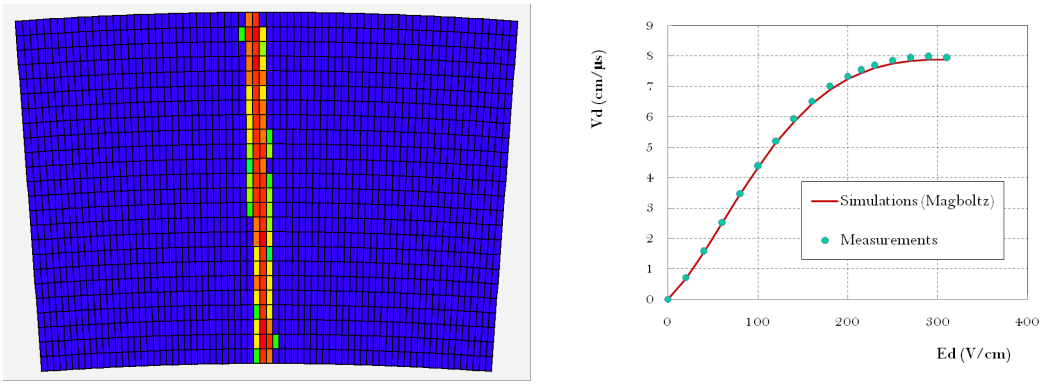

Figure 2.14: Left: A typical track from the beam. Right: Drift velocity as a function of the drift field. The dots are the measurements, the continuous line is Magboltz prediction.

Data were taken in various periods from October 2008 to March 2010. A typical beam-track display is shown in Fig. 2.14(left); the color scale codes the pulse height. This track is at 5cm drift distance, and one can see that the charge is shared on two to three pads due to the resistive foil. The detector works at a gas gain of typically 1200 to 2500. Many different conditions were varied over wide ranges with and without zero suppression to generate a very detailed series of studies: the sampling frequency, the shaper peaking time, the electronic gain and the drift length.

A measurement of the drift velocity in T2K gas as a function of the drift field is shown in Fig. 2.14(right). At a drift field of 230 V/cm, the drift velocity was measured to be 7.698 ± 0.040 cm/μs, whereas the Magboltz prediction under these experimental conditions of temperature and pressure, taking into account a measured 35 ppm water content, is 7.583 ± 0.025 cm/μs, where the error on the prediction reflects the uncertainty of gas composition. This difference is small but significant ($1.5 \pm 0.6\%$).

The uniformity of the detectors was tested as described next. Cosmic-ray tracks spanning the whole detector were used to measure the average charge deposited per track per row; it was found to be uniform over the 24 rows. Figure 2.15 shows the average displacement of the track vs the row number for data taken at B = 1 T with beam passing at the center of the detector. The average displacement of x_{track} as a function of padrow was found to be less than 20μm rms for the carbon-loaded kapton, and reached 40μm for the resistive ink module. The r.m.s. of the uniformity was 7μm for the carbon-loaded kapton, and much larger for the resistive paint. The patterns are independent of z, showing that they are due to the detector itself. The deviations in the case of resistive ink are probably due to the resistive-layer non-uniformity. In the case of resistive kapton foil, the homogeneity is found to be very good, with no edge effect or dead area up to the edge of the module observed, which is a nice achievement of the bulk Micromegas technique.

The resolution was measured as a function of the drift distance for a number of conditions. Figure 2.16 shows the resolution for B=0T (left) and B=1T (right). The resolution extrapolated at zero drift distance is 60μm for 3mm-wide pads, confirming previous results obtained with smaller prototypes (50μm and better with 2mm pads). The effective number of electrons is found to be $38.0 \pm 0.2 \pm 0.8$, where the systematic error comes from the uncertainties on the magnetic field and the input diffusion coefficient from Magboltz. This value is consistent with expected ionization fluctuations and seem to indicate that there are low gain

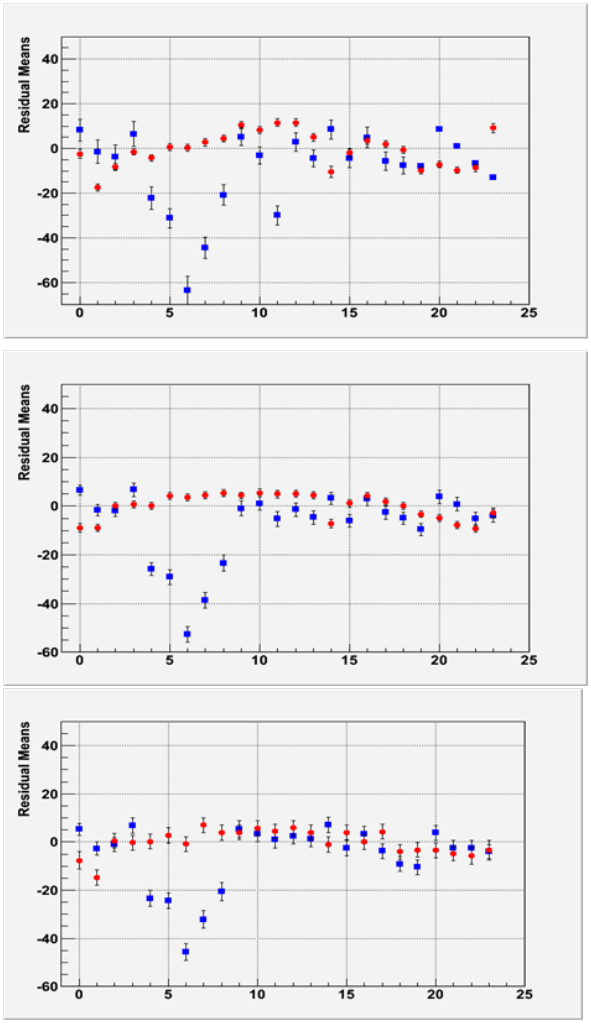

Figure 2.15: Average displacement in μm of the hit with respect to the track versus the row number, for three values of the drift distance : z=5cm (top) z=35cm (middle) z=50cm (bottom). Data points are for the carbon-loaded kapton (in red) and for the resistive paint (in blue).

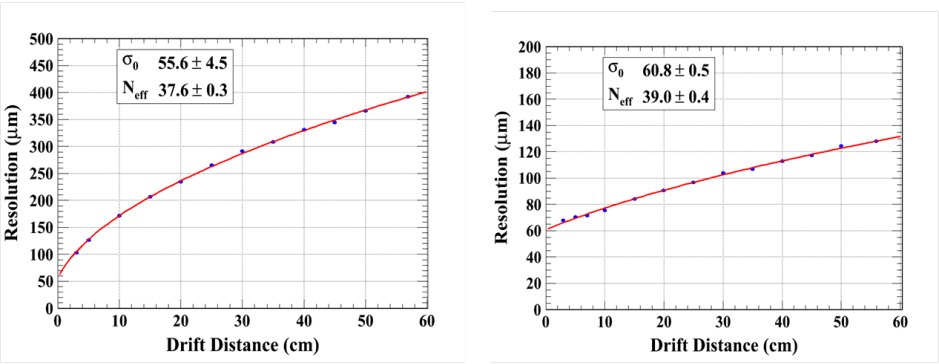

Figure 2.16: Resolution for B=0T (left) and B=1T (right).

fluctuations in the Micromegas. This is also supported by detailed studies of single electron avalanches [29] [30].

In July 2010, data were taken at CERN in a high intensity pion beam with Module 3 in its test gasbox. Even at the maximal intensity (180kHz of 150GeV pions over a region of $2\times5\text{cm}^2$) the operation was smooth, and two tracks on the same pad separated by less than a microsecond could be readily distinguished. No charge-up effect was observed at this high intensity.

2.2.3.2 Step 2: Seven-module preparations.

Carleton University and Saclay contributed to this effort on new electronics. The whole chain of readout has been subject of a new integration to accomodate all the electronics just behind the seven modules of the LP. Front-end cards were redesigned, each with four 72-channel AFTER chips, and with the naked chips wire-bonded on an eight-layer card (2cm×16cm). Most of the protection against sparks has been removed (double diodes, charge-limiting capacitors), except for (at the prototype level) current-limiting resistors. Tests on a standard T2K detector demonstrated that 15 Ohm resistors in series between the pad and the pre-amplifier suffice to protect. The resistive foil should give enough resistance for the protection of the chips. These front-end cards are connected to the PCB by two 300-point flat connectors of a new type, allowing many groundings spread among the 288 pad connections. This design minimizes the length of the connection between a pad and a preamplifier and thus the noise.

Most of the other functions are transferred to the mezzanine card, a single ADC with better resolution replaces ADCs on all the cards, and an FPGA handles the communication with the chips through an optical link. A new backend has been designed and constructed. It can handle up to twelve optically connected modules and is compatible with the EUDET TLU. This electronics is 'power-pulsing ready', as the power on the amplifier can be cycled from the mezzanine FPGA. There is a plan, in a Saclay-Carleton-Kolkata collaboration within LCTPC, to conduct power-pulsing studies in the 5T DESY magnet.

New modules have also been designed (see Fig. 2.17). A routing consistent with the high density connectors has been produced. It uses a new technique of filled buried vias, and robust solutions have been found to attach the front-end cards to the detector PCB. These techniques can also be used for GEMs and will allow a better integration, more modularity, easier maintenance and easier work sharing between teams of different labs. A new solution

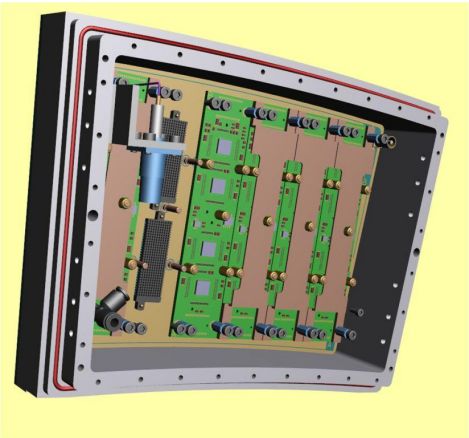

Figure 2.17: The electronics side of one of the 'Seven modules'.

for the grounding was found, after two detectors had a via destroyed by sparks; this solution consists of metallizing the resistive foil on the edges of the PCB. This also allows us to reduce the dead area on a module to zero and to get a perfect electric field up to the edges.

The complete chain should be tested at the end of 2010. Then will start the production of nine modules, using a quasi-industrial production chain followed by a characterization of each module on a testbench at CERN in 2011. At the end of this production, tests will start with seven modules mounted on the present endplate and will continue in 2012, in view of contributing to the Detector Baseline Document (Sec. 2.3).

2.2.4 LP with pixelised readout

The goal of the SiTPC task within EUDET is to provide a precision endplate structure (or module) for the highly pixelised readout of a TPC consisting of either Gas Electron Multipliers (GEMs) or Micromegas as gas multiplication devices and integrated CMOS amplifiers and digitization ASICs as a replacement of the conventional pad readout. The Universities of Freiburg and Bonn, CEA-Saclay, CERN and NIKHEF contribute to this task.

At the time of the previous PRC review in April 2008, several single-Timepix chip detector systems were produced and tested, with radioactive sources, cosmics and testbeam at DESY, either with a triple-GEM stack or a Micromegas or Ingrid (a Micromegas like grid integrated directly onto the Timepix chip using CMOS post-processing techniques). The Micromegas or Ingrid have the advantage that sufficient gas multiplication can be obtained with a single-stage device. However the high electric field (of order 80 kV/cm) just above the CMOS chip make them prone to severe damage by discharges. In fall 2007 a solution was found by covering the Timepix chip with a high-resistive protective layer of aSi:H of 20 μm thickness.

In the following sub-sections progress since the previous PRC review is described. The overall goal has been to produce and get experience with larger surface systems, composed of up to 8 Timepix chips.

2.2.4.1 Technical developments

Several PhD theses [31, 32] and journal papers on Ingrid technology developments have been produced during the reporting period (e.g. on a GEM-like structure (GEMgrid) [33]) and

on a double-stage Ingrid (Twingrid) [34]. The GEMgrid was investigated in order to obtain a mechanically much more robust structure. The Twingrid structure was developed as a possible alternative to highly-resistive protection layers, the idea being that one could either share the gas multiplication in two steps or altogether constrain the gas multiplication to the first stage (a GEM like operation), thus reducing the electric field just above the Timepix chip. Both structures were successfully operated, with gas multiplications similar or close to the one of a single Ingrid. The Twingrid structure, due to its more complicated production process, has (for the time being) not been pursued further. A similar GEMgrid structure is now under development on full 8" wafer scale, see Sec. 2.2.4.2.

A paper on discharge protection has been submitted to NIM. Another suitable material for a high-resistivity protection layer Si_3N_4 has been applied. A beam test at DESY seems to indicate that a layer of at least 8 μm thickness is needed to keep the Timepix operational over long periods.

In preparation of an LP module with 8 Ingrids, a 4-fold Ingrid/Timepix module was prepared by the Nikhef group in fall 2009. It was tested shortly at the DESY testbeam. Unexpected problems with the data acquisition are still under investigation. The plan is to replace the existing Pixelman readout by a newly developed fast readout. Recently a single Timepix/Ingrid detector was successfully read out simultaneously with the ZEUS MVD beamtelescope using common EUDAQ software.

2.2.4.2 LP with GEMs and timepix

The status of tests with GEMs combined with timepix will be be given next.

Recent studies. The groups at the Universities of Bonn and Freiburg have studied the readout of a TPC with a triple GEM-stack and Timepix chips. Test detectors with various drift lengths were used for this purpose. The Bonn group used their 26cm long TPC prototype to determine the dependence of quantities such as transverse spatial resolution, cluster size, cluster charge or number of clusters per track length on the drift distance. With cosmic ray data it was demonstrated, that the spatial resolution is very close to the diffusion limit of single electrons (see Fig. 2.2.4.2(left)). Only for drift distances below 10 cm the influence of multi-electron clusters were observed in all quantities.[35] During a test beam campaign at the local electron accelerator ELSA these results could be confirmed. Additionally, it could be demonstrated, that the transverse spatial resolution is almost independent on the track inclination (see Fig. 2.2.4.2(right)). In 2009 the setup was placed in the B = 5 T

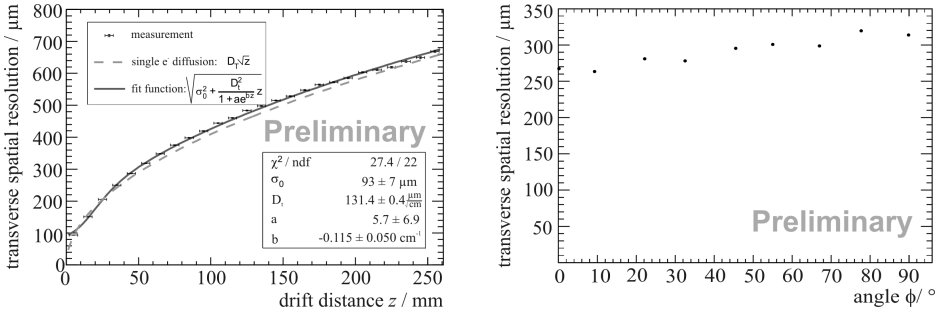

Figure 2.18: Left: Dependence at 0 T of the transverse spatial resolution on the drift distance. Right: Dependence of the transverse spatial resolution on the track inclination.

superconducting magnet at DESY, where it could be demonstrated, that the readout scheme works reliably at high magnetic fields.

A readout module for the Large Prototype at DESY was produced featuring eight Timepix chips. This module was tested with the 5 GeV-electron test beam at the EUDET facility at DESY. The previous results could be reproduced, however, the inhomogeneities of the PCMAG led to deviations at large drift distances. Therefore, a second test beam campaign is planned for the next year. These studies will then take advantage of the improved infrastructure in the test beam area.

It was realized during the analysis, that single primary electrons generate a signal, that is spread over 40-60 pixels. To reduce this number, a wafer of Timepix chips was sent to the Fraunhofer Institut IZM at Berlin, where the pixels were combined to larger pad size structure. The size of these pads vary from 2×2 to 10×10 original pixels. These post-processed chips were tested using the laser testbench at Freiburg and a hadron test beam at CERN. Both tests demonstrated that pad sizes of 110×110 μm^2 up to 165×165 μm^2 show no significant degradation in performance with respect to the original pixel size of 55×55 μm^2, while yielding significantly more charge per pixel at the same gas gain. Therefore, the gas gain can be reduced by a significant factor.

Wafer-based Production of GEMGrids. The InGrids[36] produced at the University of Twente have shown a very good behavior in many experiments. The production process, however, is based on single chips. Therefore, the production rate is rather low and can hardly satisfy the needs for R&D. Thus, a new wafer based production is being established in collaboration with the Fraunhofer Institut IZM at Berlin. To increase the mechanical stability, the GEMGrid design [33] was chosen and some slight changes in the production process were made. First samples produced on a dummy silicon wafer have been delivered and were tested at Bonn; signals generated by radioactive sources were observed.

2.2.4.3 LP with Ingrids and Timepix

A demonstrator of a digital readout for Time Projection Chambers has already been built and operated using a single Timepix and Micropattern Gaseous detector, Micromegas and GEM. However, larger surfaces need to be established before possible application in a future linear collider experiment. Given that the MUROS readout can only read eight TimePix chips at the same time, an eight-chip matrix prototype with integrated Micromegas, Ingrid, has been designed and built in Saclay. Figures 2.19 and 2.20 describe more in detail the Octopuce module which was made to fit to the large TPC prototype endplate located at the DESY testbeam facility. In order to help the handling and the wire bonding the matrix has been decoupled into a daughter board connected to the MUROS through a mother board. The latter supplies the chips using twelve voltage regulators providing protection and stable conditions at 2.2V during the operation.

The Octopuce has been tested electrically. Only nine dead columns (out of a total of 2048 columns) were found in total. A threshold equalization was done which consists of applying adjustment bits to correct the pixel-to-pixel noise dispersion. Test pulses could be sent both in Time mode and Time-Over-Threshold mode and showed proper functioning of the whole matrix.

The Ingrid (amplification structure) properties were tested in a gas box. The drift distance was 3cm. Figure 2.21 shows a cosmic ray track taken at a mesh voltage of 375V in a Helium/Isobutane (80/20) gas mixture with an acquisition time of 0.5s in Time mode. Some

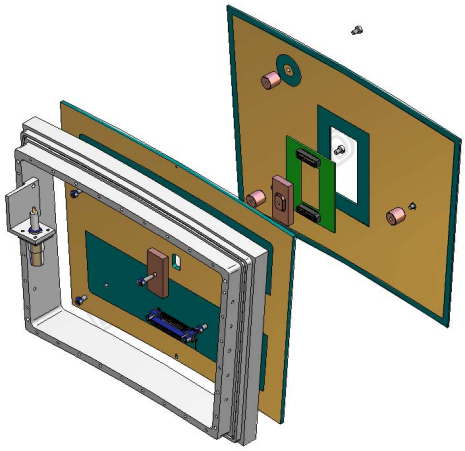

Figure 2.19: The eight chips module for the LCTPC large prototype is composed of an aluminum frame, a mother PCB, a daughter PCB and a guard plate.

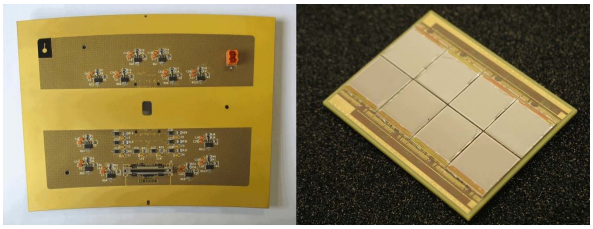

Figure 2.20: (left) Rear side of the mother board with electronic circuits for power support and readout; (right) Daughter board equipped with eight Timepix/InGrid chips.

other pictures show discharges or a current between the grid and the pixels, showing that the detector is not yet perfect. When data taking will be done in triggered mode, with short shutter opening times, the probability of seeing such discharges in the image will be very low. A second Octopuce module is in preparation.

As the Octopuce has been operated for several days under stable conditions, it is planned to be used in a beam test at the LP in DESY to detect tracks from electrons of up to 6 GeV/c.

2.2.4.4 Development of a TimePix-2 chip

Given the success of the TimePix chip, and the experience gained with Medipix-3, the Medipix Consortium (CERN) has decided to develop TimePix-2 (TPX-2). This chip will be made in 130 nm technology, will have a time resolution better than a ns, and will have a (sparse) read out system better adapted to particle physics instrumentation. The frame based readout, required for imaging, will be adapted in a variant: TPX-3.

The TDC-per-pixel, in the form of a shortly active interpolation 600 MHz oscillator has been prototyped in Gossipo-3 (a Nikhef-Bonn MultiProjectWafer collaboration), and will be the basis for the TDC of TPX-2. essentially new is that all data is stored in individual pixels. By separating the (analog) front end and the digital data processing, TPX-2 can operate with zero dead time. A fast, 'all data to shore' readout system, pionered by the LHCb collaboration, is under study. TPX-2 will include drift time and TimeOverTheshold

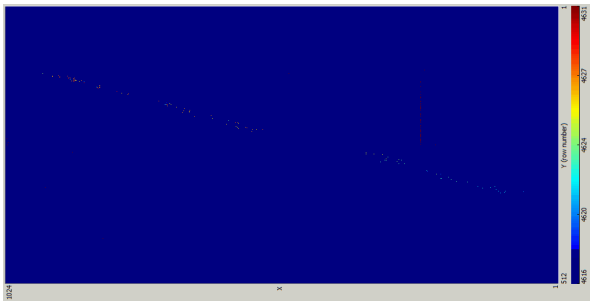

Figure 2.21: Single cosmic track in Time mode from the Octopuce in He/iC_4H_{10} (80/20) at a grid voltage of 375 V. No trigger system for cosmics was used. The acquisition time was set to 0.5s.

(ToT) per hit pixel. Per pixel, there is only room for a 4-bit 'bunch ID'. Per column, a 16 bit word can be written.

2.2.5 Other small/medium prototype studies

The results of various studies have been mentioned in several of the sections in this PRC2010 report. Here follows a list of other measurements.
- MWPC gas-amplification has been ruled out due to large E×B effects. [37]
- Ar-CF_4 mixture is a good candidate for GEM-based gas-amplification. [38]

2.2.6 Photoelectron calibration system

The photoelectron calibration system for the LCTPC is being studied at the LP.

Design. In order to monitor and correct for distortions arising from non-uniform and non-aligned electric and magnetic fields, the LCTPC fieldcage design includes a system to emit a fixed pattern of photoelectrons from the cathode surface. Comparing the image pattern with the actual pattern or with images taken under different electric or magnetic field conditions indicates the transverse displacements of electrons that traverse the full drift distance of the TPC. Should this prove to be a useful tool for the prototype TPC, it could be included in the design of the eventual LCTPC.

The cathode surface is copper-plated aluminium. A pattern of 2 mm diameter dots and 2 mm wide strips of exposed aluminum was formed by machining away copper with a numerically controlled mill. The pattern chosen is shown in Fig. 2.22(left), superimposed on the pad pattern for a single Micromegas readout module. The dot locations were chosen to be at the corners of the pads in order to improve the spatial resolution for situations when distortions were small.

Ultraviolet light of 266 nm wavelength is used in the system as it is sufficiently energetic to produce photoelectrons from aluminum, but not copper. A pulsed UV laser is used to generate a beam that is split and focused into two fibres. The fibres carry the light to the LCTPC endplate, which has two mounted optical packages which defocus the light onto the central cathode. The TPC DAQ is triggered when the laser fires, allowing the readout electronics to record the pattern of electrons. In addition to distortion studies, the arrival time of the photoelectrons allows the drift velocity to be precisely monitored.

As a goal, roughly 100 photoelectrons per dot were to be emitted, similar in amplitude to the charge collected by pads from minimum ionizing particles passing through the detector. In this way, the electronics parameters would not need to be adjusted when switching between normal data taking and calibration running.

Initial results. A typical event is shown on the right side of Fig. 2.22(right). The centre of the dot images are estimated by a likelihood fit to the observed charge shared in neighbouring pads.

A simulation of the photoelectron setup was incorporated into the LCTPC simulation. With an average of 100 photoelectrons emitted per dot, repeated measurements of the x-coordinate (horizontal direction) of a dot have a standard deviation of about 0.15 mm, when operated with T2K gas at 1 T magnetic field. For typical calibration data runs, 636 and 638, the observed standard deviation is about 0.25 mm. The resolution is somewhat worse than the prediction from simulation, but sufficient to do distortion studies, particularly since many calibration events can be recorded in a short period of time. The poorer resolution could be due to fewer photoelectron statistics.

In order to demonstrate the effects of non-uniform magnetic fields on the TPC performance, data was collected with the TPC at different locations within the magnet. When at large displacement (z=50 cm), the TPC drift volume is within a very non-uniform magnetic field. Figure 2.23 shows the difference between the locations of the dot images with the TPC at 5 and 50 cm displacement. A significant 2-D distortion pattern is easily seen. Note that it would be difficult to deduce this distortion pattern simply by collecting cosmic or beam tracks without external reference. The magnet field map data was implemented into the simulation and an attempt was made to reproduce the distortion pattern, by including the drift of electrons in a non-uniform magnetic field. As of this time, the simulated distortion pattern does not match the actual distortion, neither in the general pattern nor the magnitude. This indicates a problem with the use of the field map data or the simulation of the transport of the drifting electrons.

This preliminary analysis suggests that this calibration system will be a powerful tool to confirm our understanding of the distortions produced by the non-uniform fields in which the LCTPC is expected to operate.

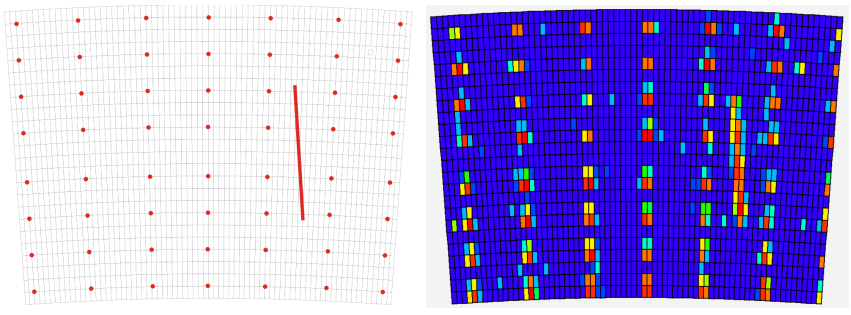

Figure 2.22: Left: The red areas indicate the original pattern of exposed aluminum on the copper cathode replicated for each readout module location. Superimposed on the image is the pattern of pads for the Micromegas readout modules. Right: The pattern of charge collected by the pads is shown for one event. The color indicates the amount of charge, with red being the largest.

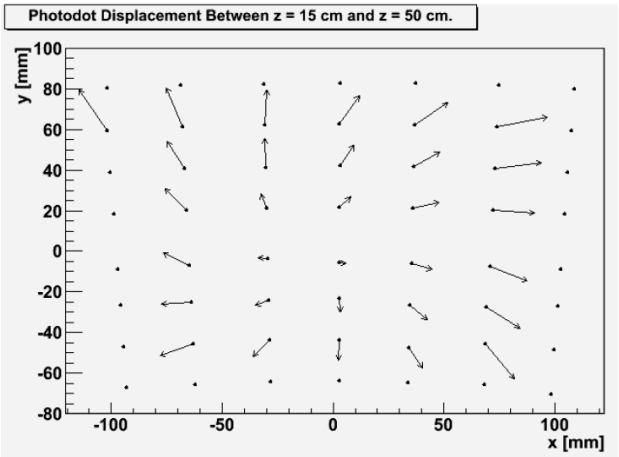

Figure 2.23: The black dots indicate the locations of the centres of the reconstructed dots when the TPC is displaced by 5 cm in the magnet (Run 638). The arrow tips indicate the locations of the centres of the reconstructed dots when the TPC is displaced by 50 cm in the magnet (Run 636). The arrows therefore give a direct indication of the additional transverse displacement of electrons when the TPC is moved into a very non-uniform region of the magnet. The dots without arrows are seen in Run 636, presumably because they are displaced outside of the active region for the module.

2.3 DBD preparations

The ILD concept should prepare a Detector Baseline Document by the end of 2012 Therefore the LCTPC collaboration meeting on 21-22 September 2009 reviewed a number of issues to prepare for the next three years of work and to be ready with its contibution to the ILD DBD in 2012.

The ILC Research Director has produced a workplan for the DBD which can be used as a guide for our preparations. Relevant for the LCTPC are the "demonstration of proof of principle on critical components, definition of a feasible baseline with options, completion of mechanical design and development of a realistic simulation." All of these points are covered in the ILD LOI [1], and further work will involve R&D priorities and design issues for the next two-to-three years.

2.3.1 Advanced endplate

Physics goals of the ILD require that design of the TPC endplate simultaneously achieves rigidity and stability while minimizing the material contribution upstream of the endcap. The requirement for rigidity and stability is driven by the momentum resolution and is covered in Sec. 1.2. The competing requirement for low scattering material in the TPC endplate is driven by the the particle-flow analysis. Recent simulations (Sec. 1.2) of the effect on reconstruction of jets in the ILD endcaps show that there is negligible degradation in the observed jet energy resolution if the endplate material is limited to about 25%X_0. Present estimates of materials in the ILD endplate are: detector elements and amplifiers, 5%; cooling, 2%; signal and power cables, 10%. The contribution from signal and power cables is achieved with expected developments in an optical fiber readout and DC-DC converters. Thus, there

remains about 8%X_0 in the material budget for the rigid mechanical structure of the endplate.

LCTPC members have been studying a series of endplate structural designs. The current LP1 prototype TPC, Fig. 2.24(left), was completed and installed in October 2008. This endplate was developed to meet the precision alignment requirement while deferring studies to meet the low-material requirement. This is a solid machined aluminum structure that

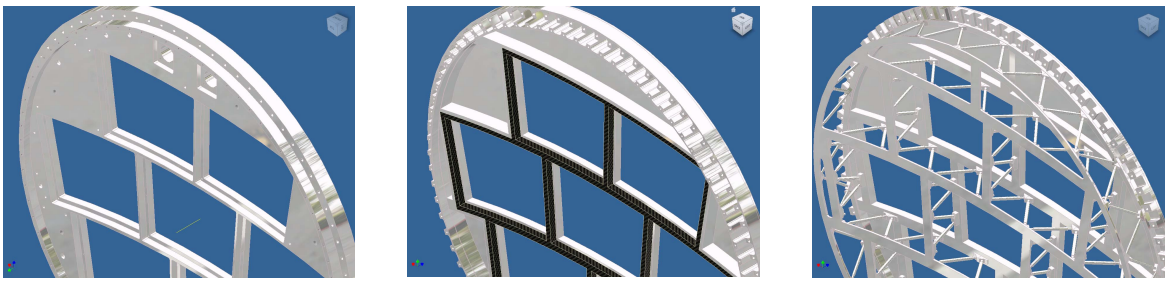

Figure 2.24: Left: The current LP1 endplate mechanical structure. Middle: Model of an LP1 endplate using hybrid construction. Right: Model of an LP1 endplate using spaceframe construction.

provides a rigid framework for supporting detector modules. Detector modules are each mounted on individual aluminum frames that mount to main structure with precision dowels located in the framework. Strength and stability of the framework, and thus the precision mounting holes, is increased with integral stiffening bars that extend away from the endplate, between the detectors. Manufacturing procedures were investigated to improve the precision and stability of the structure. The selected process employed a magnesium-silicon alloy of aluminum with three machining steps, leaving 0.75mm and 0.25mm surface material in the first and second steps. The structure was stress relieved with a liquid nitrogen shock after the first two steps. On completion, most precision features were measured to within 40μm of design; all precision features are within 75μm.

Development of an advanced endplate that meets both the precision and low-material requirements is in progress. These studies include endplate structures at three levels of R&D: the ILD endplate, replacement endplates for the LCTPC LP1 prototype, and small structures to study the mechanical details of construction techniques. The small structures will be the first to be built; they provide a comparison to finite element calculations and can be completed quickly and inexpensively before committing time and funds to an LP1 endplate.

Endplate designs will retain the current method of mounting the readout detectors in modules as is necessitated by the MPGD gas-amplification devices. Designs being considered also retain the method of locating the modules in a rigid framework. Two approaches for reducing the material while maintaining rigidity are being pursued. Both benefit from significant material reduction at the outer rim but differ in the way that material is reduced on the endplate surface.

In the first approach, material is reduced by incorporating fiber material into the machined endplate. This will result in a hybrid construction, shown in Feg. 2.24(middle), that retains the aluminum precision surfaces while replacing a significant volume of the framework, including stiffening bars, with fiber. The assembly is envisioned to be simplified by first machining the aluminum structure leaving material on the precision surfaces as in the process for the current endplate. This will be followed by molding the fiber directly in the

aluminum shell and final machining.

In the second approach, the stiffening bars are eliminated and replaced by a spaceframe structure, as shown in figure 2.24(right). The spaceframe is assembled from machined aluminum pieces. Precision alignment is accomplished by adjusting the individual struts.

To study the rigidity of these endplate designs, solid models have been built with the Inventor CAD package and are shown in the figures. Results of finite element analysis calculations predict that either design can provide a factor of 2 reduction in scattering material for an LP1 endplate; reduction from 17%X_0 to about 8%X_0 meets the ILD goal. However, the spaceframe design provides improved rigidity. The current endplate is predicted to deflect by 33μm with an applied force equivalent to a 2 mbar gas pressure. This prediction is consistent with measurements of the delivered endplate. Under the same applied force, the predicted deflection of the hybrid endplate is between 70 and 160μm, which may be sufficient. (Predictions for this model are difficult because input is needed on the properties of the fiber.) In the spaceframe design, with material spread over a greater depth, the deflection is predicted to be reduced to 23μm. Based on this alone, the spaceframe is currently the preferred design. The spaceframe design has the added advantage that it is expected to be more readily scaled up to the ILD size. The hybrid design will require more material in the stiffening bars to maintain the rigidity at the larger radius. In the spaceframe design, the rigidity can be increased by increasing the overall thickness without a significant increase in material. This is limited only by the requirements for spacing the endcap calorimeter based on the particle flow analysis. Before a decision is made on which design to develop as an LP1 endplate, we require a better understanding of how well the models represent reality.

Small beams that that are examples of each design will provide input to the calculations of the performance of the LP1 endplate designs. These have been designed as both solid models, for finite element analysis calculations, and as construction assemblies. The test parts will be manufactured and tested in the next month. These will be used to study the details of the complex structures and compare deflections to the model. The results of these tests will be used to refine the calculations.

Work has started on construction models of an LP1 endplate of each design with the goal of producing a replacement endplate for the LP1 prototype TPC using the favored design. The time scale for completion of the new LP1 endplate is one year. Work has also started on a model for the ILD endplate. This will be refined over a period of two years with input from studies of the LP1 endplate.

An example of the LCTPC design based on the R&D described above is seen in Fig. 2.25.

2.3.2 Advanced endplate granularity

As explained in Sec. 1.2, the TPC will be designed to have fine granularity. The motivation for this decision arises from simulations of the TPC occupancy due to the main sources of background[9] arising from beam-beam effects–gammas, pairs and neutrons–as a function of voxel sizes, seen in Fig. 2.26. This plot for standard electronics leads to the conclusion that, in order to reduce the background occupancy as much as possible, the voxels should be as small as possible. This is the reason for pad sizes and number of timebuckets in Table 1.1, and the resulting occpancy, presented in Fig. 1.3(left top), under nominal conditions is less than 0.1%.

The DBD preparations for the large number of electronic channels are further elaborated

in Secs. 2.3.4 and 2.3.5.

2.3.3 Fieldcage

The parameters given in the LOI for the ILD detector performance are driving the design of the fieldcage for an ILD TPC. Two requirements have to be fulfilled: low mass but a stiff and robust fieldcage which also acts as the gas vessel, and the ability to achieve very high mechanical accuracy. The construction of a large fieldcage based on two cylindrical barrels, an outer and an inner fieldcage with the required mechanical specifications is a rather ambitious undertaking. One will make use of the experience that has been collected by earlier collaborations that have built fieldcages with similar dimensions and start improvements from there.

A first approach has been made with the building of the fieldcage of the large prototype (Sec. 2.2.1). The diameter of the LP is similar to the inner fieldcage of the LCTPC. The material budget of about 1.2% radiation lengths is already approaching the design goal for the ILD TPC. If the ratio L/B with L being the length of the fieldcage and B the magnetic field strength is the same for the two, the magnitude of acceptable electric field inhomogeneities inside the TPC drift volume will also be the same. Therefore the relative mechanical accuracy specifications are similar for the LP and the ILD TPC. Based on the experience gained with the LP a preliminary design for the LCTPC fieldcage wall is being proposed.

For the ILD, a TPC is planned with a diameter of the inner fieldcage of 65cm, of the outer fieldcage of 360cm and a drift distance of 215cm. This is about 3.5 times longer than the LP. Since the magnetic field of ILD is 3.5T compared to 1T for the LP, the ratio L/B is the same for both TPCs and so are the relative mechanical-accuracy specifications. Scaling the mechanical tolerances of the LP by a factor of three yields a tolerance for the alignment of the fieldcage axis in the range of 300μm and for the parallel alignment of anode and cathode of 450μm for the ILD TPC.

The main challenge for the design of the ILD TPC will be the reduction of the material budget of the wall to 1%X_0 while increasing the high voltage stability to $\mathcal{O}$(100kV). Starting from the current LP wall cross section (Fig. 2.3), a reduction of the material budget is possible by thinning down the field strips to 20μm and by replacing copper by aluminum. In

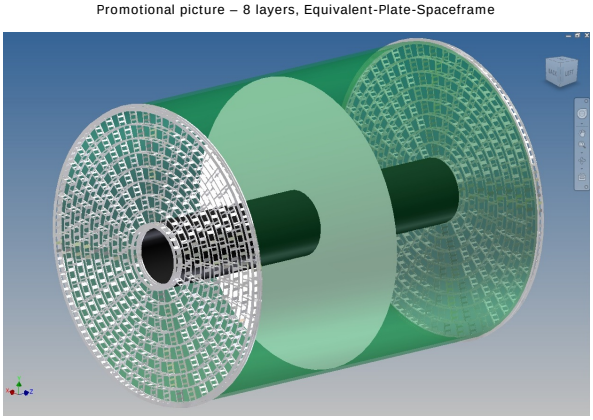

Figure 2.25: An example of a model for the LCTPC.

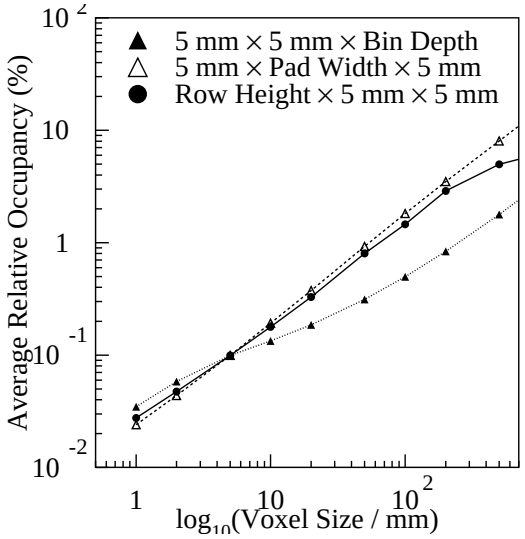

Figure 2.26: Occupancy in the TPC as a function of voxel sizes

addition, with further optimization studies of the chamber static forces and mechanical tests, the thickness of the GRP could be diminished. This would reduce the contribution of epoxy and glass-fiber to the material budget. Assuming a moderate optimization, GRP layers of 200μm could be sufficiently stable to construct a self supporting tube of 4.3m length for the inner fieldcage. The LP wall samples were tested to be high voltage stable up to at least 30kV. In the wall sample tested, a single polyimide layer of 50μm was introduced which can withstand 10kV alone. The insulating honeycomb-GRP structure increased the high voltage stability to above 30kV. Extrapolating to the ILD TPC, the wall of the inner fieldcage could have a cross section as shown in Fig. 2.3. Here, an insulation which is equivalent to a single 300μm thick polyimide layer together with the honeycomb sandwich provide a high voltage stability of around 70kV. This wall has $1\%X_0$, which is the design value. However, the detailed fabrication of the thicker polyimide layer still has to be evaluated and tested.

The outer fieldcage of the ILD TPC will be a single barrel structure serving as gas vessel and high voltage insulation. Its material budget goal is $2\%X_0$. At the same time the wall must be thicker than the one for the inner fieldcage to gain sufficient mechanical robustness. A wall thickness of 60mm, which could provide a sufficient stability, can be realized by scaling up the thickness of the honeycomb material and doubling the thickness of the GRP layers. In this case, the material would reach the design value of $2\%X_0$. It must be stated that the mechanical and the high voltage stability, both for the proposed inner and outer fieldcage wall, need to be quantified by dedicated calculations and sample tests. Also the mechanical-precision specifications have to be revisited on the basis of further studies and taking into account the final detector gas.

2.3.4 S-Altro

The goals of momentum resolution and two-track separation for the LCTPC requires having small pads; 1x4 mm^2 pads are assumed here. Thus the size of the front end electronics should not exceed this area per channel. The original plan was to mount the electronics directly onto the pad board using bump bonding to minimize the size. Preliminary studies

have shown that a bump bonded 64 channel SALTRO64 chip will have a size of about 100 mm^2, which means somewhat more than 1.5 mm^2 per channel. Including board controller, voltage regulators, optical readout and passive components it still seems feasible to meet the size requirement. However, the replacement of a malfunctioning chip is a difficult operation which will require advanced equipment and that the module be dismounted. The present prototype chip has 16 channels. Extending this to 64 channels will be an expensive step, and therefore all prototyping during the next 2-3 years should be done with the 16 channel version. The difficulties foreseen in the replacement of chips directly mounted on the pad module call for alternative solutions. An interesting option being investigated at the moment would be to place the electronics on small separate boards which are connected to the pad module via micro-connectors. Since the electronics components can be mounted on both sides of such a board a first study with wire bonded SALTRO16 chips has shown that such a design is compatible with 1x6 mm^2 pads, whereas the 64 channel SALTRO64 chip could be accommodated on a pad board with 1x4 mm^2 pads. The pad size of 1x6 mm^2 should be sufficiently small for the prototyping stage. The advantages in placing the electronics components on separate boards are listed next.

• Trace routing from the pads to the SALTRO chip becomes simpler since translational routing will only be necessary at the edges of the pad module.
• With fewer or no active electronics components on the pad board it will be easier to design.
• Changes during the electronics prototyping will be cheaper, easier to implement and test.
• The interface between SALTRO-part and the controller/readout-part is well defined. Thus in the prototyping stage one can separate the analogue and digital functions on two boards.
• This offers good possibilities to divide responsibilities for design and production between different institutes.
• The trace routing on the plug-in board will be easier compared to the trace routing in case all the electronics is placed on the pad board. The pad board will need fewer layers.
• Analog and digital functions are separated which makes it easier to optimize noise performance.
• Heat is moved away from the TPC endplate.
• It facilitates service. A malfunction in the readout chain can easily be fixed by replacing the elecronics board instead of dismounting the whole pad board.
• The readout electronics can easily be moved from one gas amplification system based on GEMs to one based on MicroMegas.

Figure 2.27(left) shows a schematic draft of a Multi Chip Module (MCM), which accommodates eight SALTRO16 chips i.e. four on each side of the board, two buffer chips for the clock distribution and passive components. The dimensions of the board are 31.5 by 23.5 mm^2, which is slightly smaller than the area covered by 32x4 pads of size 1x6 mm^2. The board is connected to the pad module via four micro connectors, which elevate the boards by 4.3 mm above the pad module and therefore enable the mounting of components also on the surface facing to the pad board. The input connectors have 40 pins (32 for signals and 8 for ground) and a pin pitch of 0.4 mm. Two 60 pin connectors provide the connection to the board controller and the LV supply respectively, which are on separate boards perpendicular to the MCM in order to facilitate cooling.

In the case of the final 64 channel SALTRO64 chip, a board with 8 chips seems to be optimal from a size point-of-view, since the buffer chips contain 8 channels each i.e. one per SALTRO64 chip. The dimensions of the chip itself have not been specified yet but for this study 12.5x 8 mm^2 has been chosen which is optimal to match the dimensions of the

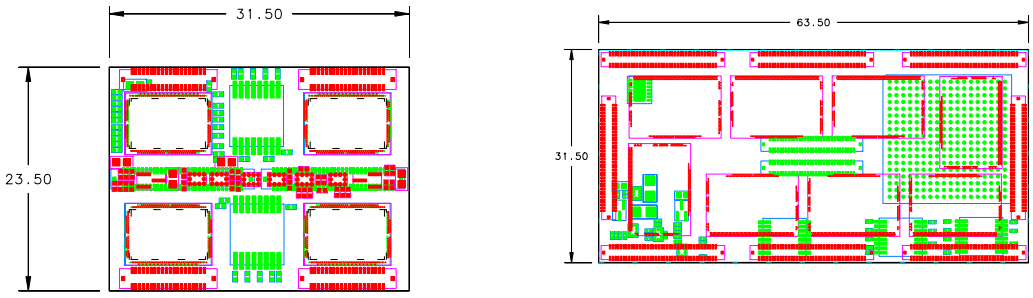

Figure 2.27: Left: the FEC-MCM for eight SALTRO16 chips. Right: the FEC-MCM for eight SALTRO64 chips. Both cases include clock buffers and various passive components. Components in read are on the board surface facing the pad module, and those in green are on the outside with respect to the pad module.

MCM. A schematic layout of such a board with wire bonded SALTRO64 chips is shown in Fig. 2.27(right). In this design all the 8 SALTRO64 chips are placed on the surface facing the pad plane together with the eight input connectors, having 80 pins each with 0.4 mm pin pitch. The rest of the electronics components are on the opposite side including the board controller, the buffer chips and the DAC. With this solution there is no need for another insertion board as in the case of the MCM design for the SALTRO16 chip. The dimensions of the board are 63.5 by 31.5 mm^2 which can be accommodated on an area covered by 64x8 pads of size 1x4 mm^2. In case that the dimensions of the SALTRO64 chip will be different and/or the size will become bigger than 100 mm^2, this can still be arranged on the MCM if the SALTRO64 chips are mounted on both sides and an additional plug-in card for the board controlling functions is introduced as in the case of the prototype MCM with the SALTRO16 chip. The connectors in the centre of the board indicate the space available for plug-in cards and the LV supply.

2.3.5 Cooling, power-pulsing studies

Beside the TPC large prototype beam tests being currently carried out at the DESY T24-1 beam line, there remains important R&D to do to realize a thin TPC endplate with the S-ALTRO readout electronics. Our original solution was to integrate the S-ALTRO readout electronics on the MPGD pad PCB to obtain minimum material thickness of the TPC endplate and to mount 64ch S-ALTRO chips directly on the backside of the MPGD pad PCB by bump bonding together with other necessary electronical components.

More recent ideas involve the use of Multi Chip Modules (MCM) attached to the pad PCB via micro-connectors (see Sec. 2.3.4). Since the MCM proposal did not exist early 2010, the direct bump-bonding idea was used to design a 'dummy board', as described in the next paragraph, to test cooling and power-pulsing which will be a part of the final scheme.

The earlier solution of direct bump-bonding was certainly very aggressive, and, beside the development of the S-ALTRO chips itself, a study of thermo-mechanical and electrical features of such an assembly will be important. Assuming a pad size of 1×4 mm^2, the density of the readout channel of the pad PCB will be 220,000ch/m^2, and the power consumption

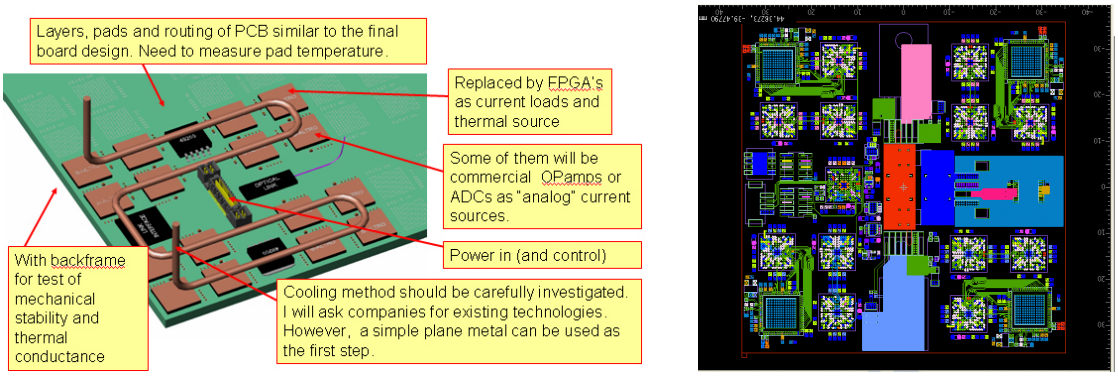

Figure 2.28: Left: Illustration of one section of the pad-board design. Right: One section of a test PCB with FPGAs, which mimic the pad PCB with the S-ALTRO readout electronics, for the test of power delivery, power pulsing, and cooling. For pads of the size of 1.1 × 4.5 mm^2, there are 12 identical sections on the test PCB.

of the S-ALTRO is estimated to be about 100W/m^2 at 10MSPS or 200W/m^2 at 40MSPS with the power switching assuming a duty cycle of 1.5%. The total material thickness of the pad PCB mounted with the S-ALTRO readout electronics is estimated to be around 5% X_0 (without cables for the low voltage supply).

We have started to build such an test-assembly of bump bonding, power delivery, power pulsing, and cooling by designing a realistic pad PCB, the 'dummy board', with bump-bonded FPGAs which replace the 64ch S-ALTRO chips as power consumers. In addition to the FPGAs, some ADCs, amplifiers, voltage regulators, optical links as well as other electrical components will be mounted. Altogether this test PCB with FPGAs will mimic the pad PCB mounted with S-ALTRO and enable us to try out the ideas. With this setup, we plan to test the 2-phase CO2 cooling which is one of the most advanced cooling methods for providing a uniform cooling (temperature) and with the minimum material of coolant and piping. We also plan to perform a test in a magnetic field to identify any problems of the Lorenz force under the power pulsing.

An illustration of one section of the pad-board design is shown in Fig. 2.28(left), and the current layout in Fig. 2.28(right). The cooling pipe in the illustration has not been optimized yet. The one section of the test board is 72 × 70.4 mm^2, and a full test board consists of 12 identical sections. The size of the pads of this test board is 1.1 × 4.5 mm^2. The test board has 10 metal layers with FR5 insulator. Out of the 10 layers 8 layers are actually used to connect the pads to the pins of FPGAs, ADCs, and amplifiers.

The design of the test board has been validated and submitted for fabrication. By November this year, after some initial tests, the boards will be mounted with the components. The first 2-phase CO2 cooling are planned for the beginning of 2011.

2.3.6 Software for Reconstruction and Simulation

Far-reaching preparations if software tools are in progress.

Motivation. At one of the forming workshops of the LCTPC collaboration, it was decided to use a common reconstruction framework so as to minimize the duplication of efforts and to provide a test bench to compare, on an equal footing, various technologies for the endcap MPGD detector modules. The result is the MarlinTPC which is based on the common

persistency framework LCIO [39] and built upon the reconstruction framework MARLIN [40]. Complementary is the usage of LCCD [41] as the standard way of providing access and storage of conditions data. The geometry description is based on GEAR [42]. MarlinTPC is designed to handle the much more complex measurement environment of the Large Prototype.

Design and goals. MarlinTPC is an implementation of a TPC data model [43], but is still incomplete since some envisaged processors and functionality are still being developed. It is a part of the highly modular MARLIN framework. The data types defined in LCIO are driven through a linear chain of software modules. These modules interact only on basis of an event. Several data types are defined for a tracker, which also outline the processing chain, listed in Table 2.2. Two main distinctions need to be made in the description of the

Type	Default Collection Name
TrackerRawData	TPCRawData
TrackerData	TPCConvertedData
TrackerPulse	TPCPulses
TrackerHit	TPCHits
Track	TPCTracks

Table 2.2: The basic data types defined in LCIO for track reconstruction in a tracking detector. The order of the data types and their (default) name outline the processing chain.

processing chain. The first is the basic reconstruction, that is anything before track level, and the second is within the basic reconstruction for the different types of data input, i.e., data from the different readout schemes, namely pixelized or pad-based data.

Basic reconstruction. The most basic unit of pad-based data is the time-binned ADC data of individual pads. These are grouped together into pulses, which are the convoluted signals on individual pads. In pad-based readout the pulses are combined row-wise into hits. These hits are the space points, calculated from the time and the charge-weighted position of the individual pulses.

Data from pixel readout has to be treated differently. Due to the small pixel size the chip can resolve individual charge clusters which are spread over several pixel-rows. This requires a 2D clustering algorithm. The Timepix chip currently used can only record either charge or time per pixel, which requires interpolation between pixels by the clustering algorithm. From the reconstructed clusters the hit positions are calculated.

The common result from the either basic reconstruction is the TrackerHit, a 3D space point including charge information and the respective errors.

Higher level reconstruction. The next step in the reconstruction chain is the track finding and fitting to form tracks from the hits. The first part is a pattern recognition which finds hits that belong together on a single track. This collection of hits is then passed to the final fitting to yield the track parameters.

Track finding and fitting is an iterative process, which needs some steering logic. Within the linear processing scheme of MARLIN this is hard to achieve without making the construction overly complicated. Some initial effort to implement track finding and fitting for single track events is available. But most of the effort for track reconstruction is put in the development of special tracking libraries, which are then called by a processor. The most important development is a tracking library based on the Kalman Filter technique.

The library KalTest [44] is based on ROOT [45] and provides basic C++ classes for track fitting with the Kalman filter technique. The library allows handling of measurement layers of various shapes and coordinate systems in a unified way so as to minimize user-implemented code. The library has been tested using test beam data from the Large Prototype TPC.

In addition there is a likelihood fitter which can find the most likely track parameters using a model of charge distribution when given a set of signal pulses. A future goal is to implement corrections into the likelihood fitter which overcome the effects of field inhomogeneities.

Correction of Large Prototype data. One of the main reconstruction goals of measurements with the Large Prototype is to develop the ability to describe and correct the large inhomogeneities in the electrical and magnetic fields.

One approach is the usage of data taken with the photoelectric system consisting of UV laser light to illuminate a dot pattern on the cathode, as described in Sec. 2.2.6. The reconstruction of photoelectric data uses the standard MarlinTPC reconstruction chain up to the pulse step. Once the pulses have been found only information from pads which have been associated with the projection of the photoelectric geometry are extracted for further analysis. Photo-dots are reconstructed using a likelihood method, it is possible to reconstruct photo-lines using another method.

Output from the reconstruction is imported into ROOT where analysis can be performed. Within ROOT it is possible to generate displacement maps to analyze the drift of reconstructed photo-dot position for different positions of the TPC. It is also possible to estimate the ability to reconstruct the positions of the photo-dots using the standard deviation of the distribution of the repeated measurements of the x-coordinate of a photo-dot.

Simulation. There are also several ways to describe the signal creation by particles traversing a TPC. Three different simulation chains are currently implemented in MarlinTPC, differing in the level of sophistication and detail. The most simple is based on the smearing of a Geant4 Hit, with the addition of some electronics simulation to provide the most basic information. On intermediate level the primary ionization is taken into account, from which charge clouds are drifted, diffused and amplified. The highest detail is provided by a simulation that takes single electrons in every stage into account. This level of detail is needed for pixelized readout, which can resolve primary charge clusters and even single electrons.

All the chains provide realistic raw data like it would come out of a prototype (or large experiment) TPC. This allows the validation of the whole reconstruction chain, from raw data to reconstructed tracks. Recently the input format for all three chains has been made compatible with MOKKA [46] output, so it can be used to test the efficiency of the reconstruction algorithms for real physics cases.

The most recent addition to the simulation is the work on the photo-dot signal creation. It is currently possible to simulate the creation of photo-electrons (assuming a uniform distribution of UV light). The drift of these electron clouds can be simulated by evolving a Langevin model of ion drift using numerical methods. Magnetic field values are provided to the simulation by 2D or 3D field maps which were generated by adding measured corrections to a perfect dipole field.

There are also several dummy data generators, that simulate pulses or hits, which are mainly for code development purposes.

Conditions data handling. The MARLIN framework allows the access and handling of conditions data by a special processor, which is common the whole framework. This "Conditions Processor" is the first in the linear chain and inserts the necessary data into the event stream. The relevant conditions data is then retrievable in any processor downstream in the

processing chain.

In MarlinTPC a collection of conditions data classes exist, which are derived from the LCGenericObject data type. These are provided in the TPCCondData, which are automatically compiled and linked with MarlinTPC. The conditions data classes can also be compiled as a separate library without dependency on MARLIN. This allows us to link it to a data acquisition program without introducing the full ILCSoft as dependency. The EUDET data acquisition (EUDAQ [47]) package implements this for the readout of the Timepix chips to automatically write the chip conditions.

Work and Organization. In total about 30 people have contributed so far to MarlinTPC; recently active are 12 of them. The code itself resides in a svn repository [48], and provides working branches for the developers and the common development (called "trunk"). It also provides the means for software releases, which are included in the general ILCSoft installation [49]. There is a project homepage [50], which is a wiki page that allows constant editing and updating of information. In addition there is a mailing list [51] and a discussion forum [52]. To complete the software communication, there is also a bug tracker [53]. There is a monthly telephone/EVO meeting where current issues are discussed and recent developments presented with regular participation from Europe, Asia and Canada.

Current status and near future plans. The TPC data model [43] itself is currently under revision, as well as the conditions data classes. Another tracking library is under development by the DESY group. A track finder based on Hough Transformations already exists, and being extended by a fitting tool. More simulations are foreseen. Work has also started to improve the current data correction and calibration methods, including, e.g., alignment.

Chapter 3

Summary and outlook

The ILD collaboration has chosen a Time Projection Chamber (TPC) as central tracker detector because of its demonstrated performance in past collider experiments. The tracking performance goals are far superior to what has been achieved at e.g. LEP and lead to a momentum resolution which is an order of magnitude better. The design goals for the TPC single point resolution are better than 100 μm in $r\phi$ and approximately 0.5 mm in rz (drift direction). With $\sim$ 200 point measurements per track this results in a transverse momentum resolution of $\delta(1/p_t) \sim 9 \times 10^{-5}$/GeV/c for the TPC only. Two-hit resolutions of $\sim$ 2 mm in $r\phi$ and $\sim$ 6 mm in rz are expected. A dE/dx accuracy of $\sim$ 5 % should be reachable.

An important goal is to have a material budget of $\sim 0.05X_0$ in r (including the outer fieldcage) and $\sim 0.25X_0$ for the readout endcaps. A jet energy resolution study showed that there was little change between endcap material of $0.15X_0$ and $0.30X_0$.

Partly within the framework of the EUDET project, a Large Prototype of a TPC was built and installed in an infrastructure consisting of the 1.25T superconducting magnet PCMAG, a movable stage at the T24 testbeam at DESY and including HV and gas supply systems together with a slow controls monitoring system.

Several measurement campaigns were held since end of 2008, with endplate readout modules of Micromegas type and of GEM type. Also a first module with triple-GEM + eight CMOS (Timepix) chips was tested at the LP; another 8-chip Timepix with integrated gas multiplication grids is prepared to be tested.

3.1 Performance summary

Recent main achievements on performance can be summarized as follows.

- The diameter of the LP fieldcage is similar to the design value of the diameter of the inner fieldcage of the ILD detector, and its actual material budget of 1.21% X_0 is already close to the design goal. An outer fieldcage of 2% X_0 is estimated to be feasible.

- Measurements with the MediTPC prototype (maximum drift 65 cm) in P5 gas at B = 4T, showed that the resolution extrapolated to full 2m drift distance would stay below 130 μm, from which one can conclude that with T2K gas the resolution goal of better than 100 μm is realistic.

- Preliminary results of the most recent beam test with three GEM modules on the LP endplate ($\sim$ 7000 channels, with pad widths $\sim$ 1.2 mm), in T2K gas and B = 1T,

showed a single-point resolution extrapolated to zero drift distance of $\sim 60\mu$m and at larger drift distances a result in agreement with a diffusion constant as expected from Magboltz. This expectation will result at 3.5T in resolutions within the design goal of $< 100\mu$m.

- Five different modules with Micromegas and 3 mm wide pads, with and without resistive coating, have been tested as single modules on the LP. At B = 1T and with T2K gas, resolutions were achieved compatible with the expectations from Magboltz and a zero-drift resolution term of 60 μm, which is comparable to the results from the GEM-modules.
- Pixelised readout using CMOS Asics has been shown to work, both with GEMs and Ingrids (integrated Micromegas-like grid) as gas multiplier, allowing the detection of single-electron clusters. Currently an 8-chip system using the Timepix chip has been tested; systems of size of the LP module are being planned.

3.2 Outlook

Current work by the LCTPC Collaboration is a continuation of the R&D on technologies and on an advanced endcap, where mechanics, electronics and power pulsing are critical issues.

- The present LP endplate has a material budget for the mechanics of 17%X_0. Two alternative designs are under consideration that reduce this to 8%: a hybrid design where a significant fraction of the aluminum frame is replaced by carbon fiber and another approach where the stiffening bars of the current design are replaced by a space frame. The latter provides much improved rigidity compared to the hybrid design.
- Efforts have started on the design of the inner and outer field cages for the ILD TPC. The goal is to achieve a 1% material budget for the inner field cage and 2% for the outer field cage, at the same time assuring sufficient mechanical robustness and HV stability.
- A 16-channel S-Altro-16 chip in 0.13 μm CMOS technology has been designed and submitted as part of a multi-project-wafer engineering run. A Multi-Chip-Module accomodating eight S-Altro chips is being designed. Ultimately, a 64-channel S-Altro-64 chip will be developed.
- R&D on pixelized readout will be continued. A successor to the Timepix chip, Timepix-2, is in its detailed design stage, and studies for large-scale wafer-based production of integrated gas-amplification structures are being carried out with industry. The mid-term goal is the production and test of a fully equipped LCTPC module for the LP.
- Cooling and power-pulsing studies are foreseen. We plan to test 2-phase CO2 cooling. A realistic test assembly of a PCB with FPGAs (which are substitutes the future S-Altro-64 chips) is under construction. A first CO2 cooling test will be carried out early 2011. Power-pulsing tests are foreseen to be performed at high B-field (e.g. in the 5T superconducting magnet at DESY)
- Significant software development for simulation and reconstruction is ongoing, both for use of analysing LP data as well as for tracking and physics studies using the full-sized LCTPC at ILC or CLIC.

Bibliography

[1] The ILD Concept Group. The International Large Detector Letter of Intent. http://www.ilcild.org/documents/ild-letter-of-intent, 2010.

[2] M. Gruwe. Gas studies for the TPC of a detector for the future Linear Collider. LC-DET-1999-003,http://www-flc.desy.de/lcnotes, 1999.

[3] M.T. Ronan. Time-projection chambers. PDG Particle Physics Booklet, page 264, 2006. See also http://instrumentationcolloquium.lbl.gov, Time_Projection_Chamber_R&D.pdf.

[4] Y. Giomataris et al. Micromegas: A High Granularity Position Sensitive Gaseous Detector for High Particle Flux Environments. Nucl. Instrum. Meth., A376:29, 1996.

[5] F. Sauli. GEM: A New Concept for Electron Amplification in Gas Detectors. Nucl. Instrum. Meth., A386:531, 1997.

[6] A. Raspereza. Contribution to the Sim/Reco session at LCWS2007, Desy Hamburg 29 May - 4 June 2007. http://www-zeuthen.desy.de/ILC/lcws07/pdf/Sim_Reco/raspereza_alexei.pdf, 2007.

[7] Mark Thomson and Steve Aplin. TPC Endcap X_0 Study. to be published in the DBD, 2012.

[8] Steve Aplin. Study of the TPC Endcap Mechanical Thickness. to be published in the DBD, 2012.

[9] A. Vogel. Beam-Induced Backgrounds in Detectors at the ILC. PhD thesis, Department Physik der Universität Hamburg, 2008.

[10] LCTPC Groups. TPC R&D for an ILC Detector. LC-DET-2007-005, http://flcweb01.desy.de/lcnotes, 2007.

[11] LCTPC Collaboration. TPC R&D for a Linear Collider Detector, Status Report April 2008 to the DESY PRC65 meeting, http://prc.desy.de/sites/site_prc/content/e38/e60/e126/ infoboxContent130/PRC65-TPC_report_31March2008.pdf. 2008.

[12] ALICE Collaboration. A Large Ion Collider Experiment, ALICE TPC - Technical Design Report. CERN, Geneva CH, ISBN 92-9083-155-3, 1999.

[13] EUDET Collaboration. The EUDET facility at DESY, http://www.eudet.org/newdesign/. 2008.

[14] M. Dixit et al. Position sensing from charge dispersion in micro-pattern gas detectors with a resistive anode. Nucl. Instrum. Meth., A518:721, 2004.

[15] Proposal PRC R&D-01/03 to the DESY Physics Review Committee. LC Note LC-DET-2002-008, http://www-flc.desy.de/lcnotes, 2003.

[16] STAR Collaboration. STAR TPC, http://www.star.bnl.gov/. 2009.

[17] P. Schade. Correction Methods for TPC Operation in Inhomogeneous Magnetic Fields. LC-DET-2010-001, http://www-flc.desy.de/lcnotes, 2010.

[18] Daniel P. Peterson. Presentation at LCWS07 tracking session, http://www.lepp.cornell.edu/ dpp/linear_collider/ILC_Presentations.html. 2007.

[19] R. Settles and W. Wiedenmann. The Linear Collider TPC: Revised Magnetic-field Requirements. LC-DET-2008-002, http://www-flc.desy.de/lcnotes, 2008.

[20] R. Settles and M. Thomson. Suggestion for Amount of Alignment-Data Needed. See replies linked at http://acfahep.kek.jp/subg/ir/bds/ilc-bds.html#mdi: Q15(Z-pole), 2008.

[21] LCTPC Collaboration. Website for the LCTPC collaboration. http://www.lctpc.org, 2007.

[22] Ties Behnke et al. A Lightweight Field Cage for a Large TPC Prototype for the ILC. arXiv:1006.3220 [physics.ins-det], Preprint DESY-10-084, June 2010, accepted for publication in JINST, 2010.

[23] T. Lux. Studies for a Time Projection Chamber for the Internationnal Linear Collider and Measurement of Beauty Cross Section in Deep Inelastic Scattering at HERA. PhD thesis, University of Hamburg (2005), DESY-THESIS-2005-019, 2005.

[24] M. E. Janssen. Performance Studies of a Time Projection Chamber at the ILC and Search for Lepton Flavour Violation at HERA II. PhD thesis, University of Hamburg (2008), DESY-THESIS-2008-011, 2008.

[25] M. Kobayashi. An estimation of the effective number of electrons contributing to the coordinate measurement with a TPC. Nucl. Instrum and Methods A 562 (2006) 136, 2006.

[26] M. Kobayashi et al. Performance of MPGD-based TPC prototypes for the linear collider experiment. Nucl. Instrum and Methods A 581 (2007) 265-279, 2007.

[27] L. Hallermann. Analysis of Gem Properties and Development of a Gem Support Structure for the IlD Time Projection Chamber. PhD thesis, University of Hamburg (2010), DESY-THESIS-2010-015, 2010.

[28] D.C. Arogancia et.al. Study in a beam test of the resolution of a Micromegas TPC with standard readout pads. Nucl. Instr. and Meth. A 602 (2009) 403, 2009.

[29] T. Zerguerras et al. Single electron response and energy resolution of a Micromegas detector. Nucl. Instr. and Meth. A 608 (2009) 397-402, 2009.

[30] M. Lupberger. Avalanche statistics and single electron counting with a TimePix-InGrid detector. Diploma Thesis, Freiburg University, September 2010, 2010.

[31] M. Chefdeville. Development of Micromegas-like gaseous detectors using a pixel readout chip as collecting anode. PhD thesis, University of Amsterdam (NL), 2009.

[32] V.M. Blanco Carballo. Radiation Imaging Detectors Made by Wafer Post-processing of CMOS Chips. PhD thesis, University of Twente (NL), 2009.

[33] M. Chefdeville M. Fransen H. van der Graaf C. Salm J. Schmitz J. Timmermans V.M. Blanco Carballo, Y. Bilevych. GEMGrid: a wafer post-processed GEM-like radiation detector. Nucl. Instr. and Meth. A 608 (2009) 86-91, 2009.

[34] M. Chefdeville M. Fransen H. van der Graaf C. Salm J. Schmitz Y. Bilevych, V.M. Blanco Carballo and J. Timmermans. TwinGrid: A wafer post-processed multistage Micro Patterned Gaseous Detector. Nucl. Instr. and Meth. A 610 (2009) 644-648, 2009.

[35] C. Brezina et. al. A Time Projection Chamber with triple GEM and pixel readout. JINST 4 P11015, 2009.

[36] M. Chefdeville et al. An electron-multiplying Micromegas grid made in silicon wafer post-processing technology. Nucl. Instrum. Methods, vol. A556, pp. 490, 2006.

[37] K. Ackermann et.al. Cosmic Ray Tests of the Prototype TPC for the ILC Experiment. http://arxiv.org/pdf/0905.2655v1.pdf, 2009.

[38] M. Kobayashi et.al. Cosmic ray tests of a GEM-based TPC prototype operated in Ar-CF4-isobutane gas mixtures. http://arxiv.org/pdf/1008.5068v1, submitted to NIM, 2010.

[39] LCIO Homepage. http://lcio.desy.de.

[40] MARLIN Homepage. http://ilcsoft.desy.de/marlin.

[41] LCCD Homepage. http://ilcsoft.desy.de/lccd.

[42] GEAR Homepage. http://ilcsoft.desy.de/gear.

[43] TPC Data Model. http://www.desy.de/∼wiene/marlintpc/tpcdatamodel.pdf.

[44] KalTest Homepage. http://www-jlc.kek.jp/subg/offl/kaltest/.

[45] RooT Homepage. http://root.cern.ch.

[46] MOKKA Homepage. http://polzope.in2p3.fr:8081/MOKKA.

[47] EUDAQ Homepage. http://projects.hepforge.org/eudaq/.

[48] MarlinTPC repository (public access). https://svnsrv.desy.de/public/marlintpc/.

[49] ilcinstall Homepage. http://ilcsoft.desy.de/ilcinstall.

[50] MarlinTPC Homepage. https://znwiki3.ifh.de/MarlinTPC/.

[51] MarlinTPC mailing list. ilcsoft-marlintpc@desy.de.

[52] Linear Collider Forum sub forum Tracking & Vertexing. http://forum.linearcollider.org/index.php?t=threadt&frm_id=39.

[53] Software issue tracker. https://jira.slac.stanford.edu/browse/MAR.